Master thesis

Towards renewable fuels

The effect of upscaling on catalysts used for bio-oil upgrading

Author
L.M. de Kort, BSc.

Supervisors
Dr. Pieter Bruijnincx
Dr. Gareth Whiting
Ir. Ana Hernández Giménez

Inorganic Chemistry and Catalysis
Utrecht University

December 1, 2017

Abstract

This thesis aims to elucidate the effect of upscaling on K-grafted USY catalysts used in the gas-phase aldol condensation of propanal, which is chosen as model reaction for the upgrading of bio-oil. Technical extrudate catalysts are obtained via extrusion of USY zeolite with a clay binder, either attapulgite or bentonite, followed by a K-grafting procedure.

The effect of this upscaling procedure on the physicochemical properties of the catalysts was studied with several characterization methods, including ICP-OES, XRD, Ar physisorption, CO_2- and Py-IR studies and CFM-based techniques. K-grafted USY/Attapulgite and USY/Bentonite extrudates were successfully synthesized given that the physicochemical properties of the parent USY material are largely preserved after upscaling. In both cases, the inclusion of clay results in the incorporation of active sites originating from the binder material. Upon K-grafting, additional active sites are created in attapulgite-bound extrudates, whereas active sites are removed from the bentonite-bound catalyst.

Catalytic performance was studied with *operando* FT-IR/DRS-UV-Vis and *in-situ* FT-IR/DRS-UV-Vis measurements combined with on-line MS and off-line GC, respectively. It was found that the inclusion of binder results in an increased activity accompanied by a reduced selectivity and stability. Upon K-grafting, the overall performance of the technical catalysts improves. The trends in performance correlated with the changes in active sites observed during both steps of the upscaling procedure. Hence, it is concluded that the upscaling procedure has a significant effect on the technical catalyst properties and performance.

Contents

Chapter 1

Introduction

1.1 Production of second-generation biofuels

In years to come, renewables will play a key role in meeting the world's energy needs. In particular, because the progressive depletion of conventional fossil fuels calls for an increased use of renewable energy sources. The importance of renewable energy sources is even reflected in international energy regulations. The EU's Renewable energy directive has set the target of final energy consumption from renewable sources at 20% by 2020, which will then be raised to 27% as part of the EU's energy and climate goals for 2030. Additionally, by 2020 each EU country is required to obtain at least 10% of their transport fuels from renewables.[1] Luckily, a wide variety of sources, such as biomass, wind, solar and hydropower, can be used to generate energy as heat and power and thereby meet the energy consumption targets. However, although several renewable sources can be used for energy generation, biomass is currently the only renewable source of carbon that can be converted into liquid fuels, that can be used as fuel for an internal combustion engine.[2]

Biomass conversion

Many types of biomass feedstocks are available for the production of biofuels. Currently, research is focussed on biofuel from lignocellulosic biomass (wood and agricultural waste amongst others) called second generation biofuel. In contrast to the biomass source used for first generation biofuel, i.e. sugars and vegetable oils, lignocellulosic biomass can be grown on non agricultural lands or in combination with food, thus without competing with food production.[2–4] For that reason, lignocellulosic biomass has been proposed as a better candidate for the sustainable production of biofuels.

Several thermo-chemical conversion processes have been developed to convert biomass feedstocks into liquid products, generally called bio-oils.[2,3] These thermal degradation processes include liquefaction, gasification, and pyrolysis.[3] The pyrolysis conversion process is defined as thermal degradation of biomass in the absence of air or with very limited amount of oxidizing agents. The process involves short residence times, fast heating rates, high temperatures and low pressures.[2–4] An effective biomass conversion with high liquid yields (70 - 80 %) and a high fuel-to-feed ratio can be achieved. This makes pyrolysis one of the most promising routes to produce second-generation biofuels that can compete with and eventually replace non-renewable fossil fuel resources.[3,5]

Bio-oil upgrading

The resulting pyrolysis oil is a complex mixture of more than 300 different oxygenated hydrocarbons, including carboxylic acids, aldehydes and alcohols, among others. Table 1.1 shows a comparison of the composition of bio-oil and crude oil. Mainly due to the highly oxygenated character and high water content of bio-oils, they obtain some properties that are undesirable for fuel applications, such as a low heating value, corrosiveness, immisciblility with crude oil and thermal and chemical unstablility.[2–6] These properties prevent the application of pyrolysis oil in mixtures with traditional fossil fuels. A general decrease in the oxygen content is necessary in order to increase the quality of the final product, thereby producing biofuels suitable for application in the current transportation system.[2,4]

Table 1.1: Comparison between bio-oil and crude oil. Reproduced from ref. [4].

	Bio-oil	Crude oil
Water [wt%]	15 - 30	0.1
pH	2.8 - 3.8	N.A.
C [wt%]	55 - 65	83 - 86
O [wt%]	28 - 40	< 1
H [wt%]	5 - 7	11 - 14

The development of efficient routes for the deoxygenation of crude pyrolysis oils is one of the primary challenges in the sustainable production of second generation biofuels. As a consequence, reaction pathways for the upgrading of bio-oil have become an important research area. Of the generally proposed upgrading reactions, especially hydrodeoxygenation (HDO) has shown very promising results.[2,4,5,7] HDO is a high pressure operation where oxygen is removed from the bio-oil as H_2O using hydrogen as feedstock. During the reaction process pressures between 75 and 300 bar, high residence times and intermediate temperatures (250 - 450 °C) are applied.[4] A high grade oil product is obtained with significantly reduced oxygen content (< 5 wt%) and a heating value equivalent to that of crude oil. Despite the increased quality of the HDO upgraded bio-oil, the high hydrogen consumption that is required hampers industrial implementation of this upgrading reaction.[2,6,8] On top of that, a large number of small aldehydes and ketones become unusable for liquid fuels, thereby decreasing the carbon efficiency of this process.[9]

Proposed cascade process

In order to overcome the challenges arising during the upgrading of pyrolysis oil to second generation fuels a cascade deoxygenation process has been proposed. Scheme 1.1 shows a schematic overview of the proposed production path from lignocellulosic biomass to second-generation biofuel. During this process, biomass is firstly converted into crude bio-oil via pyrolysis. Subsequently, the obtained pyrolysis oil is subjected to catalytic deoxygenation. In the final step a HDO upgrading procedure is used to obtain second generation biofuel. The intermediate catalytic deoxygenation step exploits the intrinsic reactivity of the bio-oil components to eliminate oxygen as water or carbon oxides via condensation reactions. The upgrading of pyrolysis oil through these condensation reactions enables oxygen removal without hydrogen consumption, while simultaneously converting the low molecular weight fraction in pyrolysis oil into heavier molecules.[6,8,9] This can reduce the H_2 usage in the additional HDO step by ca. 50% and preserves the carbon content from the small aldehydes and ketones.[6,9]

This study focuses on the catalytic deoxygenation step of the proposed cascade production path. In the following section an elaboration on this step and the relevant condensation reactions will be given.

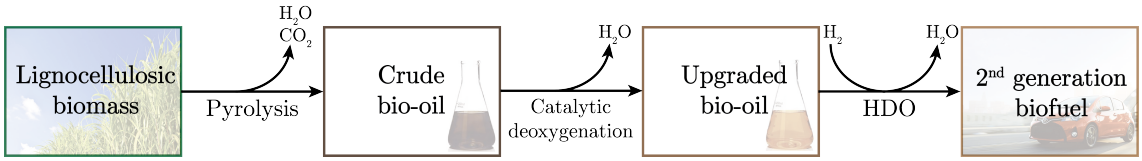

Scheme 1.1: Potential scheme for the production of second-generation biofuels from lignocellulosic biomass. Adapted from ref. [8].

1.2 Catalytic deoxygenation

The goal of the catalytic deoxygenation process step is two-fold: first of all, the oxygen content in the bio-oil should be decreased to improve its miscibility with fossil-derived fuels; secondly, the carbon chain length of the low-boiling fraction aldehydes and ketones should be converted into gasoline- and diesel-range compounds, to increase the carbon efficiency of the overall process.[6,8,9]

The intermediate deoxygenation utilizes the reactivity of the bio-oil constituents to eliminate oxygen through condensation reactions as esterification, ketonization, and aldol condensation.[6,8–11] In the latter aldehydes and ketones with an α-hydrogen atom undergo a carbonyl condensation reaction, thereby increasing the carbon chain length of the product. Subsequently, oxygen is eliminated as water in a final dehydration step.[12,13] Since short-chain aldehydes and ketones account for a large fraction of crude bio-oil (up to 25%), this makes the aldol condensation reaction particularly interesting for catalytic deoxygenation.[14,15] An example of the self condensation of an aldehyde is shown in Scheme 1.2.

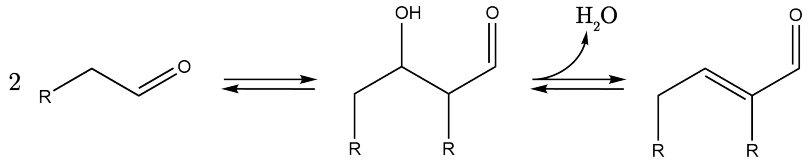

Scheme 1.2: Reaction pathway of the aldol condensation reaction of a general aldehyde. Adapted from ref. [12].

The aldol condensation reaction can be both acid- and base-catalyzed. In the base-catalyzed reaction pathway an aldehyde is deprotonated to form an enolate ion upon reaction with a base. This enolate ion can attack a second aldehyde to form an alkoxide ion, which will be protonated again. This intermediate is dehydrated and the final condensation product is formed. The acid-catalyzed reaction starts with the formation of an enol, which reacts with an protonated carbonyl to form the same intermediate.[12,13]

Potential catalyst materials

Both strong acid and base materials can catalyze a number of undesirable side reactions in bio-oil. Hence, it is important to discuss the type of catalytic materials that are most suitable for intermediate deoxygenation via the aldol condensation reaction. Historically, aldol condensation reactions have been catalyzed by homogeneous acids and bases, but current literature has focused more on heterogeneous catalysts.[9] Typically, strong solid base catalysts are proposed, such as hydrotalcites, alkaline earth metal oxides and alumina-supported alkali metal salts. However, these traditional solid bases strongly bond to adsorbed species, leading to undesired side reactions and quick deactivation due to coke formation.[6,9,16,17] Therefore, to minimize these undesirable reactions, a moderate base catalyst might be more suitable for carrying out the aldol condensation, involved in the bio-oil upgrading process. Fortunately, a number of catalysts with intermediate basic strength that yield stable performance for the condensation reaction have been identified.[6,8]

In the search for the most promising catalyst for intermediate deoxygenation, the complex nature of pyrolysis oil poses a challenge. Due to this complexity, it is difficult to study and rationalize the performance of a catalyst in this step of upgrading process. Therefore, in the development of reaction processes using real biomass as feedstock, model compounds are often selected to study catalytic performance in an initially simplified but representative system.[18] The performance of catalysts used for the upgrading of bio-oil via aldol condensation reactions can be studied with an aldehyde as model compound given that light aldehydes are among the most abundant oxygenated compounds present in pyrolysis bio-oil.[18] In this study, propanal is chosen as model compound as it is the shortest aldehyde that is liquid at room temperature, which makes it the most convenient model compound to study the upgrading of bio-oil.

The main reaction pathways that occur in the gas-phase conversion of propanal over base catalysts are shown in Scheme 1.3. Through the intented aldol condensation reaction pathway the aldol dimer (2-methyl-2-pentenal) and aldol trimer (2,4-dimethyl-2,4-heptadienal) are formed. Additionally, 3-pentanone can be formed via the Tishchenko reaction and subsequent ketonization in the undesired pathway.[13,17] Recently, it was discovered that mild base zeolites show excellent activity in the gas-phase conversion of propanal, with a 90 % selectivity to the desired pathway.[8,19]

1.3 Base zeolites

Zeolites are of great importance for catalysis, due to the unique combination of their ordered micropore network, large surface area and tunable active site structure.[19–21] It is therefore no

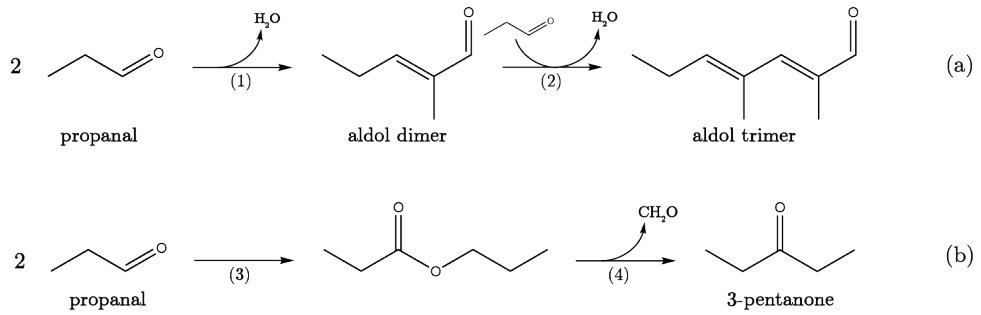

Scheme 1.3: (a) Desired[12,13] and (b) undesired[8,17] reaction pathways for the gas-phase conversion of propanal over basic catalyst via (1) self condensation, (2) cross aldol condensation, (3) Tishchenko reaction and (4) ketonization.

surprise that they have also been investigated in-depth as catalysts for condensation reactions. This interest arises mainly from the remarkably selective character of zeolites.[8]

The shape of the internal pore structure of a zeolite can strongly affect this selective character.[22] The zeolite structure is determined by the elementary building blocks, SiO_4 and AlO_4 tetrahedra. Adjacent tetrahedra are linked at their corners via a common oxygen atom, which results in an structurally unique three-dimensional zeolite framework.[20,22] The net formulae of the tetrahedra are SiO_2 and AlO_2^-, which demonstrates that one negative charge is created at each aluminum containing tetrahedron. This important for the creation of active sites, which will be discussed in more detail later. The way the adjacent tetrahedra are linked, determines the final structure of the zeolite. Many different zeolite structures can be synthesized, each with a distinctive three-dimensional framework. For example, if 24 tetrahedra are linked together as shown in Figure 1.4, a sodalite unit or β-cage is formed. When these sodalite units are connected via their hexagonal faces, this results in the faujasite (FAU) pore structure. The synthetic X and Y zeolites are FAU zeolites. Their pore system consists of spherical cages, referred to as supercages, with a diameter of 1.3 nm connected tetrahedrally with four neighboring cages through channels with a diameter of 0.74 nm formed by 12 tetrahedra.[20]

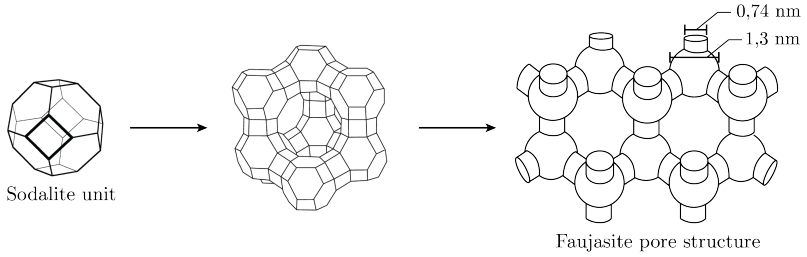

Figure 1.4: Faujasite framework building blocks and resulting micropore system including micropore dimensions. Adapted from ref. [20].

The selective character of zeolites arises from the dimensions of their micropores, which have the same dimensions as most molecules involved in the catalytic reactions zeolites are applied in. When the selectivity of a heterogeneously catalyzed reaction depends on the pore architecture of the microporous catalyst, this is called shape-selective catalysis.[20] There are several types of shape-selectivity. Reactant shape selectivity arises when reactants have larger dimensions than the channels in the zeolite and are therefore not able to enter the pore system. If a certain transition state is favored over another due to the limited space in the zeolite framework, this is called transition state selectivity. In the last type, product shape selectivity, molecules formed in the framework that are relatively large will have a limited diffusivity to reach the end of the pores.[21,22] These forms of shape-selectivity arising from the zeolite pore structure largely determine the catalytic performance of a zeolite catalyst.

In addition to the zeolite framework, the nature and strength of the active sites are determining factors for the catalytic performance as well. In general, active sites are created when the negative framework charge arising from aluminum containing tetrahedra in the zeolite framework is compensated by a cation. Changes in the Si/Al ratio will influence the density of negative framework

charges and therefore the density and strength of the generated active sites. For many catalytic applications, Brønsted acid active sites are required to initiate the reaction. In zeolites these sites are created when the framework charge is balanced by a proton. A schematic representation of the nature of this active site, a bridging hydroxyl group formed by the proton and a framework oxygen in a AlO_4 tetrahedron, is shown in Figure 1.5a.[20,23,24] Several types of Lewis acid sites, or electron acceptor centers, can be created. The precise chemical nature of these sites is less clear. Lewis acid sites mainly arise from charge-balancing extraframework cations, such as alkaline and alkaline-earth cations, and extraframework aluminum species Al^{3+} removed from the zeolite framework.[25] Basic zeolites are usually obtained by introducing exchangeable extraframework metal cations in aluminum-rich faujasite zeolites X and Y.[25,26] The introduction of the cations not only creates Lewis acid sites, but conjugated acid-base pairs are formed with framework oxygens close to the cations. A schematic representation of the nature of this active site is shown in Figure 1.5b.

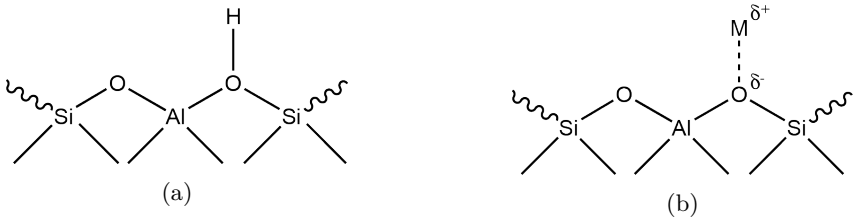

Figure 1.5: Schematic representation of a (a) Brønsted and (b) cation exchanged Lewis acid site.

The average oxygen charge, and thus basic strength, depends on the structure and chemical composition of the zeolite. It increases with aluminum content and with the size of the cations.[25–27] As a result excessive loadings of costly alkali metal cations, such as Cs^+, are needed to obtain sufficient catalytic activity from these basic zeolites.[8,28] This hinders the application of these catalysts in the upgrading of bio-oil, especially because of the cheap products that are obtained. Luckily, it has been demonstrated recently that using a simple alkaline grafting treatment, high-silica zeolites with basic sites of moderate strength can be generated. The amount of generated basic sites is even higher than expected based on the Al content.[8,19,28]

Alkali-grafted zeolite Y

In the recently discovered alkaline-grafted zeolite Y a new secondary type of basic site is formed. These sites are created through a metalation process in which silanol groups present at defect sites in the zeolite are deprotonated in methanolic solutions of the alkali metal hydroxide. The deprotonated groups are then able to coordinate alkali cations from the solution, thereby forming a new type of basic site. The overall process is shown in Figure 1.6.[19]

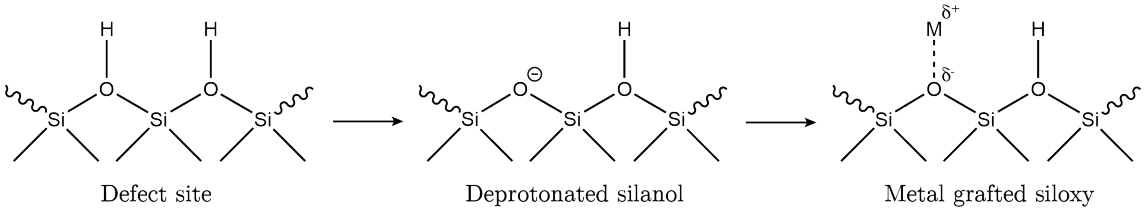

Figure 1.6: Schematic representation of the metalation process of high-silica zeolites. Based on ref. [19].

Several techniques, including magic-angle-spinning NMR spectroscopy and CO_2-TPD, suggested that the alkali metal cations graft to deprotonated silanol groups and forms basic siloxy sites.[8,19] Density functional theory (DFT) calculations made it possible to elucidate the structure of the secondary type of basic site in more detail. It became clear that different types of defects are present in USY zeolites as a consequence of the hydrothermal synthesis, which results in a number of environments where alkali cations can graft to. For several of these sites the adsorption of CO was modelled as is shown for K-grafted zeolite Y in Figure 1.7. The grafted atoms are coordinated to at least two oxygen atoms, thereby stabilizing the local environment. IR spec-

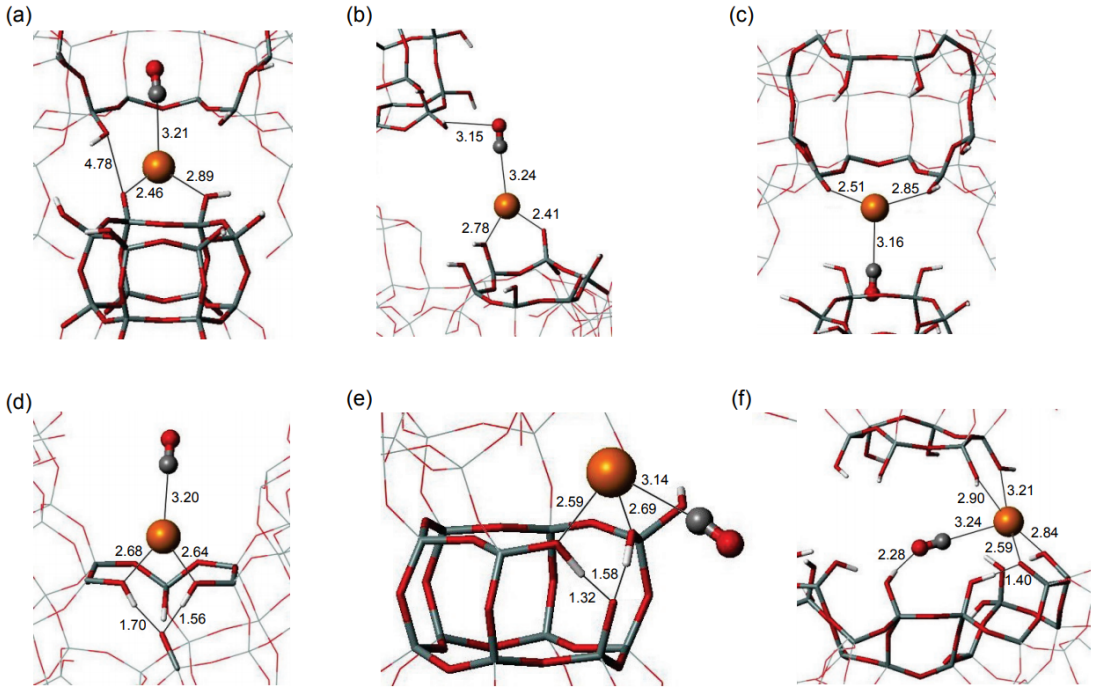

Figure 1.7: CO adsorption complexes formed on K^+-sites in K-grafted USY zeolites. Si, O, H en K are coloured in gray, red, white and orange respectively. All distances are indicated in Å. Reprinted with permission from Keller et al. [28]. Copyright (2016) American Chemical Society.

troscopy measurements confirmed that indeed multiple types of these sites were present in the grafted zeolites.[28]

The excellent catalytic performance of the alkali-grafted zeolites in the gas-phase self condensation of propanal is attributed to the presence of these basic sites.[8,19] It was found that the generation of isolated basic sites of intermediate strenght while preserving the crystallinity of the catalyst is needed to obtain highly active, selective and stable catalysts. Alkali-grafted high-silica ultra-stable Y (USY) zeolites grafted using different amounts of Li, Na, K, Rb and Cs all exhibited approximately 90% selectivity to the aldol condensation pathways in the gas-phase conversion of propanal. The aldol condensation dimer was found as main product, although even the aldol trimer was also formed at higher conversions. The catalytic performance of these catalysts remained stable over 2 hours time-on-stream. The catalyst treated with 0.1 M KOH in methanol yielded the most active catalyst with yields of the aldol condensation products approaching 40 %. Moreover, this catalyst was remarkably stable, even over 10 hours time-on-stream.[19] These promising results encourage the application of K-grafted USY as catalyst for the intermediate deoxygenation of pyrolysis oil in the proposed cascade process towards the production of second-generation biofuels.[8,19]

1.4 Catalyst upscaling

Second generation bio-fuels should be produced on an industrial scale to be able to directly compete with and eventually replace fossil-derived fuels. The scaling-up of the proposed cascade process is therefore a very important step towards the production of renewable fuels.[29] Scale-up is often an obstacle in the successful application of new catalytic technologies, because it gives rise to many new challenges. One of these challenges is the preparation of an industrial catalyst.[30] Research catalysts usually consist of a bulk or supported active phase in powder form, as is the case for the K-grafted USY catalyst proposed in the previous section. In contrast, technical catalysts are often millimetre-sized bodies composed of multiple components that should not only reproduce the performance of their research parent material, but must also have the mechanical strength and chemical stability, among other properties, required for their application in industrial reactors.[30,31]

To incorporate the needed physical, chemical or mechanical properties, technical catalysts can consist of several additives, such as a binder or porogen, complementary to the active phase. These additives can make up a major part of the final catalyst, even up to 90 %. Aside from the selection of the appropriate catalyst formulation, i.e. type and proportion of the active phase and additives, turning a promising research catalyst into a technical body involves the shaping of catalyst powders into macroscopic forms.[30] Both the chosen structuring method and formulation can severely impact the material's catalytic properties.[30,31]

Catalyst shaping

The size and shape of industrial catalysts have influence on the catalytic activity, internal and external mass transport, mechanical particle resistance and the pressure drop in large scale reactors.[32,33] Unfortunately, these properties are not all influenced by the shape of the catalyst in the same manner or at the same extend. For example, catalytic activity can be increased by a small particle size, while the pressure drop can be minimized by a large catalyst body. Thus, the optimal catalyst shape should be a compromise between the different demands, depending on the reaction conditions and reactor dynamics.[33]

For the shaping of powder catalysts into technical catalyst bodies several shaping methods can be used, e.g. pelletisation, granulation and extrusion. All structuring processes have three steps in common. Firstly, the powdered raw materials are mixed into a well-defined feed after which this pre-mixture is agglomerated into particles of the desired shape, called 'green' bodies. Finally, these shaped bodies are hardened to obtain the required mechanical strength, usually with thermal treatment.[30] Extrusion is the most economic and commonly applied shaping technique.[32] During this process a paste consisting of the active phase and the chosen additives is passed through a profiled die that determines the shape of the green body. The transportation and deformation of the paste in the die usually require high pressures. The strings formed when pressing the paste through the die are cut into extrudates of the desired length by a cutting device mounted at the extruder. The obtained green bodies are dried and subsequently calcined. During the final calcination step, mechanical strength is provided to the catalyst bodies through the formation of solid-state bridges between the particles in the extrudate. These bridges can be formed either by condensation of surface hydroxyls, thereby yielding oxygen bridges, or by sintering.[32]

Binder effects

For materials that exhibit poor self-binding properties (e.g. zeolites), the inclusion of binders is essential for attaining durable bodies with the required strength and attrition resistance.[30] Very often binders are (incorrectly) labelled as inert, even though zeolite-binder interactions can have a substantial impact on the catalytic performance.[30,31,34,35] In addition to their primary role in improving the mechanical stability, binders can impact the performance by other physical and chemical means, such as the entrapment of poisons, modification of catalyst porosity and transfer of chemical species.[30,35] The impact that binders have on industrial zeolite catalysts was recently highlighted by Hargreaves et al.[35] In this section we will focus on the reported effects of the clay materials employed in this study, i.e. attapulgite and bentonite clay.

Attapulgite and bentonite are natural clays commonly employed as binder to increase the mechanical strength of a technical catalyst upon hardening.[30] As is the case for clays in general, both clays are a source of mobile alkali and alkaline earth cations (Table B.2). These ions can exchange easily with Brønsted and Lewis acid sites in a zeolite framework, thereby modifying the activity of the catalyst.[35] Many changes in catalytic activity in attapulgite- and bentonite-bound technical catalysts are related to this solid-state exchange between the binder and the zeolite phase. For example, the surface acidity of zeolite Y and mordenite pellets was shown to decrease by the inclusion of attapulgite and bentonite clays as binder. This is ascribed to solid state migration of cations present in the clays to the zeolite extraframework sites upon pelletization.[36] Several studies on the incorporation of bentonite as binder in technical mordenite, β and ZSM-5 zeolite catalysts used in *n*-paraffins hydroisomerization also show a strong decrease in acidity due to a solid-state ion exchange between the zeolite protons and sodium cation present in bentonite.[37–39] In most cases this results in a decreased conversion, however in β zeolite catalysts the additional incorporation of extraframework aluminum species improves the *n*-paraffin conversion.[37,38] Furthermore, incorporation of bentonite provides meso- and macroporosity, which considerably improved the selectivity towards branched products.[37,39] In MFI zeolite extrudates used for the conversion of methanol to

hydrocarbons (MTH) the incorporation of attapulgite as binder significantly affected the catalytic performance as well. While a decrease in Brønsted acidity due to ion exchange between the zeolite framework and attapulgite reduced the intrinsic activity of the catalyst, a surprising increase in cycle time and light-olefin selectivity was seen. This increase was linked to the partial ion exchange with mobile Mg^{2+} species present in attapulgite.[40]

It is apparent that the choice of binder can severely impact the activity, selectivity and stability of the industrial catalysts. However, little is known about zeolite-binder interactions and how they alter the material properties, and thereby the catalytic performance.[30,31,34] Since the impact of the binder can be significant, analysis of the changes originating from the binder material is very important to increase the efficiency of industrial processes.[30]

Proposed upscaling process

The upscaling procedure shown in Scheme 1.8 has been proposed to transform the promising K-grafted USY research catalyst into a technical catalyst body that can be used in a large scale reactor. In the first step of this process USY powder, attapulgite or bentonite clay and water are mixed together to form a paste. Subsequently, this paste is extruded by pressing it through a die. The strings that form are cut into extrudates of the desired length. Finally, once the USY/clay extrudates are dried and calcined, they are subjected to a K-grafting procedure to create the desired base sites. Through this upscaling procedure a technical K-grafted USY/clay catalyst with the required mechanical strength needed in an industrial reactor is acquired.

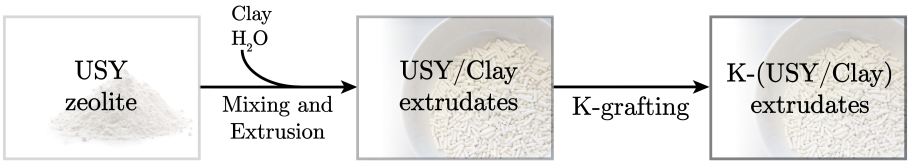

Scheme 1.8: Two-step upscaling procedure proposed for the preparation of technical K-grafted USY/Clay extrudates used in the upgrading of pyrolysis oil.

1.5 Research goal

The research goal of this project can be derived from the background information provided in the previous sections. As discussed, a novel multi-step process for the sustainable production of second generation biofuels was introduced. Application of this process on the industrial scale is important for the commercial viability of biofuel. However, upscaling of catalytic processes often creates additional challenges, including for the preparation of a technical catalyst body. Hence, it is crucial to understand the opportunities that formulation and structuring can bring to the function of these industrial catalysts. Improved rationalization will lead to great benefits in the upscaling of research catalysts to their technical form. Studying the effect of upscaling on catalysts is therefore of great scientific and industrial importance.

The main goal of this project is to add to the current scientific knowledge by studying the effect of upscaling on K-grafted USY catalysts used in the upgrading of bio-oil. This aim can be divided in two research topics, namely concerning how the material properties and catalytic performance are affected. After studying both topics, a connection between the changes in material properties and catalytic performance can be established.

Several characterization techniques will be utilized to gain in-depth information on the catalytic systems of interest. The catalytic performance of the catalysts will be studied using *operando* and *in-situ* Fourier Transform Infrared spectroscopy (FT-IR) and Diffuse Reflectance Ultraviolet-Visible spectroscopy (DRS-UV-Vis) measurements. Additionally, a number of characterization techniques, including CO_2- and pyridine-IR spectroscopy and staining techniques followed *in-situ* by Confocal Fluorescence Microscopy (CFM), will be used to give more insight in the changes in material properties of the technical catalysts.

Chapter 2

Experimental methods

2.1 Catalyst materials

An overview of the catalytic systems under study, along with their main characteristics, is given in Table 2.1. Most catalyst samples were synthesized and provided by partners within the CAS-CATBEL project, ETH Zürich and IMDEA Energy Institute. Additional catalysts were purchased or prepared during the project. Both the provided and the prepared samples were obtained using the same experimental methods.

The technical extrudate catalysts were prepared by mixing USY zeolite with the relevant clay in a 70 wt% USY: 30 wt% clay ratio using a Caleva Mixer Torque Rheometer 3. A thick paste was formed by drop-wise addition of water. Using a Caleva Multi Lab equipped with extruder attachment (0.5 mm dieplate) this paste was extruded. The formed cylinders dried overnight, after which they were cut into 20 mm extrudates. These extrudates were calcined in static air at 550 °C (5 °C min^{-1}) for 2 hours.

After preparation the catalysts were K-grafted by immersion into a 0.1 M solution of KOH in methanol for 10 minutes, in case of the powder catalyst, or 30 minutes, for extrudates. After washing with methanol the catalysts were dried at 65 °C and calcined at 550 °C for 5 hours for powders, and 2 hours in the case of extrudates.

All materials were submitted to the same conditions for drying and calcining. This was also the case for the purchased materials, i.e. high-silica USY zeolite obtained in protonic form from Tosoh Corporation (HSZ390HUA, Si/Al = 405) and bentonite clay obtained from the Clay Minerals Society(CMS) (SWy-3, Na-rich).

Table 2.1: Overview of the catalysts under study.

Nomenclature	Components	Shape	Provider
USY	Zeolite USY	Powder	Tosoh Corporation
K-USY	Zeolite USY	Powder	ETH, Imdea
K-(USY/Att)	70 wt% USY, 30 wt% attapulgite clay	Extrudate	ETH, Imdea
Att	Attapulgite clay	Extrudate	ETH, Imdea
(USY/Ben)	70 wt% USY, 30 wt% bentonite clay	Extrudate	Synthesized
K-(USY/Ben)	70 wt% USY, 30 wt% bentonite clay	Extrudate	Synthesized
Ben	Bentonite clay	Powder	CMS

2.2 Catalyst characterization

Several techniques were used for basic catalyst characterization. With ICP, SEM-EDX, XRD and Ar physisorption measurements the structural and textural properties such as crystallinity, morphology and elemental composition of the catalyst samples were studied. Pyridine-IR, CO_2-IR, CO_2-TPD and CFM were employed to study the nature, amount, strength and distribution of acid and basic sites in more detail. Insight in the distribution and the amount of deactivating carbonaceous species in spent samples was provided by CFM and TGA-MS.

ICP-OES

Inductively Coupled Plasma Optical Emission Spectrometry (ICP-OES) measurements were performed by the GeoLab on a Spectro Arcos ICP-OES equipped with a Paschen-Runge spectrometer. Emission corresponding to K, Mg and Al was measured. Prior to analysis the catalyst samples were destructed using HF and diluted using a 1 M HNO_3 solution.

SEM-EDX

Scanning Electron Microscopy (SEM) was performed on a FEI Helios nanolab 600 DualBeam microscope. The electron beam was operated at 2.00 kV at a current of 0.20 nA. The images were obtained from the secondary electrons with a dwell time of 1 µs. Energy-Dispersive X-ray spectroscopy (EDX) mapping was performed using an Oxford instruments silicon drift detector X-Max energy dispersive spectroscopy with an electron beam at 15.00 kV and a current of 0.80 nA. Prior to SEM measurements samples were prepared by placing a vertically cut extrudate on a sample holder with the cross section facing upwards and coating this with Pt in a Cressington 208 HR sputter coater using a Pt target. Sputtering was operated at 0.08 mbar Ar atmosphere with an applied current of 40 mA. The samples were rotated at a slight tilt to obtain a homogeneous layer of Pt. The coating was done for 200 s resulting in a layer of circa 10 nm.

XRD

X-Ray Diffraction (XRD) patterns were obtained at room temperature from 5 to 90 $2\theta^\circ$ with a Bruker-AXS D2 Phaser powder X-ray diffractometer using a cobalt Kα 1,2 ($\gamma = 1.79026$ Å) source, operated at 30 kV. A step size of 0.05 $2\theta^\circ$ and a scan speed of 1.0 s were applied.

Ar physisorption

Textural properties of the materials were studied by Ar physisorption measurements at -196 °C using a Micromeritics Tristar 3000. The BET method was applied to calculate the total surface area. The t-plot method was applied to obtain the micropore volume and external surface area. The Barret-Joyner-Halenda (BJH) model was used to determine the size of the mesopores.

Pyridine-IR

Fourier Transform Infrared (FT-IR) measurements after pyridine adsorption (Pyridine-IR) were performed with 16 scans per spectrum on a Perkin Elmer System 2000 with a DTGS detector and a resolution of 4 cm^{-1}. Approximately 15 mg of the catalyst were grinded and pressed into a self-supporting wafer (ø= 12 mm). The obtained sample was placed into the measurement cell. The catalyst was first dried in the cell under vacuum using a temperature ramp of 5 °C min^{-1} to reach a temperature of 550 °C. This temperature was then kept constant for 1 hour, after which the sample was cooled down to 30 °C.

Once this temperature was reached, pyridine vapors ($\sim$ 11 mbar, RT) were allowed into the measurement cell and onto the catalyst. After equilibration for 30 minutes, the cell was set under vacuum ($\sim 10^{-5}$ mbar) for 5 minutes to remove physisorbed pyridine from the sample. Subsequently, desorption was started by applying a temperature ramp of 5 °C min^{-1} to 550 °C. During the temperature program, IR spectra were taken every 25 °C to study thermal pyridine desorption.

CO_2-IR

Fourier Transform Infrared (FT-IR) measurements during CO_2 adsorption and subsequent desorption (CO_2-IR) were performed with 16 scans per spectrum on a Perkin Elmer System 2000 with a DTGS detector and a resolution of 4 cm^{-1}. Approximately 15 mg of the catalyst was grinded and pressed into a self-supporting wafer (ø= 12 mm). The obtained sample was placed into the measurement cell. The catalyst was first dried in the cell under vacuum using a temperature ramp of 5 °C min^{-1} to reach a final temperature of 550 °C. This temperature was then kept constant for 1 hour, after which the sample was cooled down to 30 °C.

Once this temperature was reached incremental doses of CO_2 were allowed on the sample. The interaction of CO_2 with the catalyst was monitored by taking IR spectra between the doses of CO_2. Subsequently, desorption was started by decreasing the pressure gradually until vacuum was reached. The desorption was monitored by taking IR spectra every desorption step.

CO_2-TPD

Adsorbed Carbon Dioxide Temperature Programmed Desorption (CO_2-TPD) measurements were performed on a Micrometritics ASAP2920 apparatus. Approximately 100 mg of sample were dried in-situ by flowing He (50 mL min^{-1}) while a temperature ramp of 10 °C min^{-1} up to 550 °C was applied. After this temperature was held for 2 hours, the sample was cooled to 50 °C. Once cooled, CO_2 was allowed onto the sample, by pulsing CO_2 until the catalyst was saturated. Desorption was started, by flushing with He flow (50 ml/min) for 1 hour and subsequently heating the sample to 550 °C (10 °C min^{-1}) to induce the desorption of CO_2. For the calculation of the number of basic sites, it was assumed that only one molecule of CO_2 can adsorb on a single site.

CFM

Confocal Fluorescence Microscopy (CFM) experiments were performed on a Nikon Eclipse 90i confocal microscope with a 100 X 0.73 NA dry objective in reflectance mode. These experiments were performed on extrudate shaped catalysts. During experiments an extrudate was placed in an open in-situ cell (Linkam Instruments, FTIR 600) equipped with a temperature controller (Linkam TMS 93). Excitation light was provided by four laser lines; 404, 488, 561 and 642 nm. The microscope was equipped with a Nikon A1 scan head. Depending on the property of interest, the samples were treated differently prior to and during microscopic analysis. The different experimental conditions used for each investigated property are summarized in Table 2.2. For the analysis of catalyst deactivation fluorescent carbon deposits present in spent extrudates obtained from the catalytic measurements were studied, while for the analysis of the acid sites fresh extrudates stained prior to the measurement as shown in Table 2.2 were visualized by CFM.

Table 2.2: Experimental conditions used during CFM experiments in which different properties are studied.

Property	Sample preparation	Fluorescent probe	Temperature (°C)
Acid sites (L+B)	*In-situ* synthesis (15 μL)*	Fluorescein	200 (10 °C min^{-1})
Catalyst deactivation	-	Carbon deposits	RT

*For in-situ fluorescein synthesis, 0.5 mL of 2M resorcinol and 1 mL of 0.2 M phthalic anhydride solutions were mixed and filled to 5 mL with absolute ethanol to obtain a 5:1 resorcinol-phthalic anhydride molar ratio. Prior to analysis the sample was stained with this solution.

TGA-MS

Thermogravimetric Analysis (TGA) was performed with a Perkin Elmer Pyris 1 TGA thermogravimetric analyzer coupled to a Pfeiffer Vacuum Omnistar MS spectrometer. Approximately 10 mg of spent catalyst was used for this analysis. An air flow (60 mL min^{-1}) was employed during thermal treatment, which consisted of heating the sample from 50 °C up to 800 °C with a ramp of 10 °C min^{-1}. During desorption the MS detector monitored H_2O, CO and CO_2.

2.3 Catalytic performance

The catalytic performance of the different catalyst samples was studied using *operando* FT-IR/DRS-UV-Vis measurements and *in-situ* FT-IR/DRS-UV-Vis measurements combined with on-line MS and off-line GC, respectively. After reaction, spent catalysts were characterized *ex-situ* using TGA-MS and CFM as described in the previous section.

2.3.1 *Operando* FT-IR/DRS-UV-Vis measurements

In an *operando* set-up combining simultaneous Fourier-Transform Infrared (FT-IR) and Diffuse Reflectance Ultraviolet-Visible (DRS-UV-Vis) spectroscopy with on-line Mass Spectroscopy (MS), the aldol condensation reaction of propanal over the different catalytic materials was monitored. The experimental set-up is schematically illustrated in Figure 2.1. FT-IR spectra were recorded on a Bruker Tensor 27 equipped with an internal DLaTGS detector. The spectra with a spectral resolution of 4 cm^{-1} were obtained by collecting 32 scans over a region from 4000 cm^{-1} to 400 cm^{-1}. Simultaneously, DRS-UV-Vis spectra were collected by an AvaSpec-2048L using an Ava-Light DH-S-BAL optical fiber. The scanning region was from 230 to 900 nm. The DRS-UV-Vis probe was positioned at the same spot as the IR beam. On-line MS data was obtained with an Omnistar Pfeiffer Vacuum mass spectrometer with quadrupole detector. The data was recorded using Quadstar 32-Bit.

Note that MS measurements do not allow for quantitative analyses, given that most of the species give rise to similar mass fragments (Table A.3). Therefore, complementary off-line GC measurements were performed for quantitative analysis of the catalytic performance (vide infra).

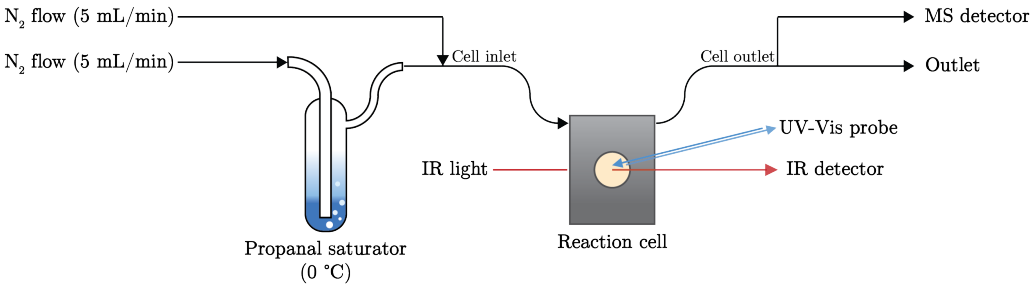

Figure 2.1: Experimental set-up used for combined FT-IR and DRS-UV-Vis spectroscopic *operando* measurements with on-line MS.

Catalyst samples were prepared by grinding the material and pressing into a self-supporting wafer (ca. 15 mg, ø= 12 mm) by applying a pressure of 30 MN m^{-2} for 20 s. The obtained sample was placed in the reaction cell. Before reaction, the sample was activated under O_2-flow (10 mL min^{-1}, Linde, 99.999%) at 150 °C (10 °C min^{-1}) for 30 minutes and subsequently at 400 °C (10 °C min^{-1}) for an additional 30 minutes. Following the activation, the flow was switched to the carrier gas N_2 (10 mL min^{-1}) for 30 minutes. The reaction was started by flowing part of the N_2 gas flow (5 mL min^{-1}) through a propanal-containing saturator kept at constant temperature of 0 °C. The other part of the N_2 gas flow (5 mL min^{-1}) was flushed for dilution of the reactant stream. After 1 hour of reaction, the propanal flow was stopped. Finally, The reaction cell was flushed with N_2 (10 mL min^{-1}) for 40 minutes.

2.3.2 *In-situ* FT-IR/DRS-UV-Vis measurements with off-line GC

For *in-situ* FT-IR/DRS-UV-Vis measurements combined with off-line Gas Chromatography (GC) the experimental set-up as discussed in the previous section and shown in Figure 2.1 was used with a few small adjustments. The adjusted experimental set-up is schematically illustrated in Figure 2.2. During these measurements the cell outlet is not connected to a mass spectrometer, but to a cold trap kept at constant temperature of -196 °C. The contents collected in this cold trap are analyzed *ex-situ* by GC-MS, for identifying the species, and by GC, for quantitative analysis.

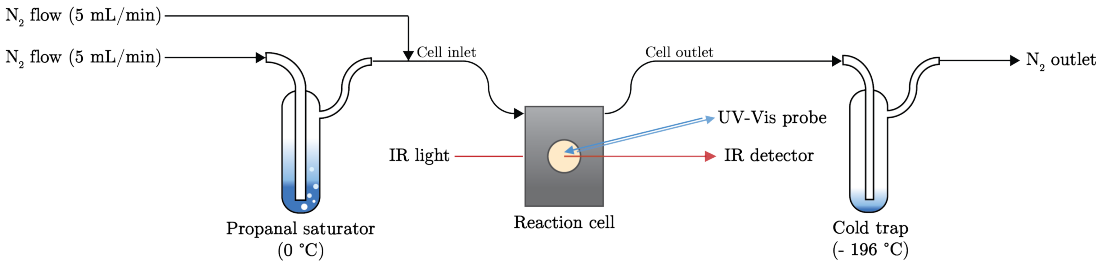

Figure 2.2: Experimental set-up used for combined FT-IR and DRS-UV-Vis spectroscopic *in-situ* measurements with off-line GC analysis.

For both the *in-situ* and the *operando* measurements identical procedures for sample preparation, activation, reaction and desorption were used. In case of *in-situ* FT-IR/DRS-UV-Vis measurements with off-line GC, the outlet line was connected to the cold trap after activation and prior to reaction. This line was disconnected immediately after reaction and just before desorption. The condensed products were collected with 0.6 mL 1,4-dioxane as solvent and placed in a GC sampling vial for analysis.

GC experiments were performed on a Varian 430-GC Chromatograph with a VF-5MS column (30 m, 0.25 mm, 0.25 μm) equipped with a Varian CP-8400 autosampler. GC-MS experiments were performed on a GCMS-QP2010 Shimadzu apparatus with a similar column equipped with an AOC-20i auto-injector. For all measurements the same program was used. The injector temperature was set at 270 °C with column flow of 2.0 mL min^{-1}. FID detector was set at 300 °C. After the stabilization time of 1 minute, the temperature of the column was kept constant at 40 °C for 3 minutes after which it was increased to 290 °C (20 °C min^{-1}).

From the chromatograms obtained during GC experiments propanal conversion, X, was calculated using $X = 1 - \frac{n_{out}}{n_{in}}$. Here, n_{out} is the molar amount of propanal collected in the cold trap during 1 hour of reaction and n_{in} is the molar amount of propanal inserted in the reaction cell. The conversion was normalized by the amount of propanal converted during reaction at 400 °C for 1 hour in the absence of a catalyst (blanc reaction) and the catalyst weight.

Chapter 3

Results and Discussion

As discussed in chapter 2, several characterization techniques have been employed to study the effect of upscaling on K-grafted USY catalysts. In this chapter the results obtained using these techniques will be discussed in detail. For this purpose, the material properties of the individual catalysts are reviewed, after which these results will be connected to the catalytic performance of the catalysts.

Both the choice of the clay and the K-grafting procedure have a large impact on the catalytic performance of the catalyst. This is exemplified in Figure 3.1, as large differences in propanal conversion are observed for the different catalytic materials. Note that the propanal conversion is only one parameter for the overall performance of the materials. The different contributions to the total catalytic performance, e.g. activity, selectivity and stability, will be unraveled in the following sections. Firstly, the effect of K-grafting on the research catalyst USY is explained. Following, the results obtained for the technical catalysts prepared with both clay materials are discussed individually. In the final section, the trends observed for the individual clays will be compared and explained.

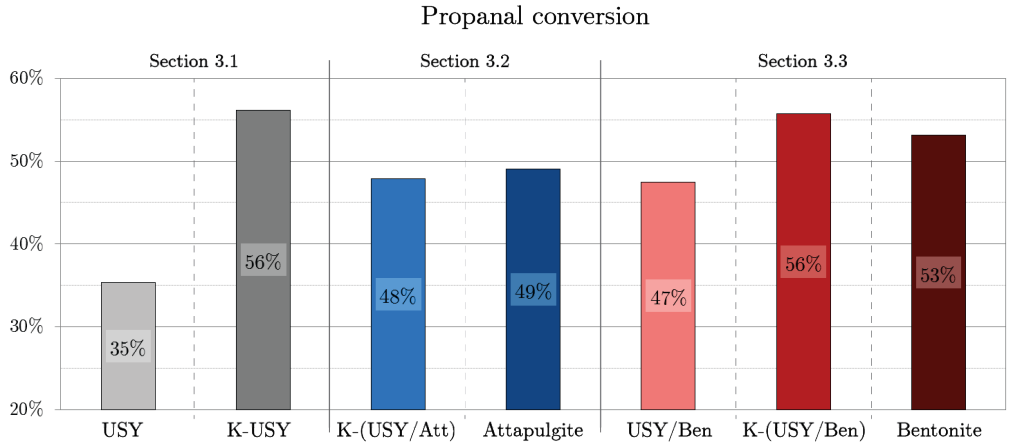

Figure 3.1: Comparison of the propanal conversion, X, obtained during *in-situ* FT-IR/DRS-UV-Vis measurements with off-line GC for the catalysts that are discussed in sections 3.1, 3.2, and 3.3. As explained in section 2.3.2 the conversion was calculated using $X = 1 - \frac{n_{out}}{n_{in}}$ and normalized.

3.1 Research catalyst

In this section the effect of K-grafting on the research catalyst USY will be discussed. Firstly, the effect of K-grafting on the general material properties is analyzed using ICP-OES, IR spectroscopy, XRD and Ar physisorption. Following, the nature of the basic and acid sites present in the catalyst before and after K-grafting is elucidated using CO_2- and Py-IR. Finally, the impact on the catalytic performance of the catalyst is studied.

3.1.1 General characterization

The aim of the K-grafting procedure is to incorporate potassium in the USY zeolite structure. It is confirmed with XRF that 0.075 mol K per mol Si is introduced in the catalyst, which amounts to 4,87 wt% K.[19] Additionally, Keller et al. found that during the grafting process the potassium cations graft to deprotonated silanol groups, as illustrated in Figure 1.7.[28] This is confirmed by IR spectroscopy, as seen in Figure 3.2a, where the IR absorbance in the OH-stretching region is shown for both the non-grafted USY and grafted K-USY catalyst after activation. The band at 3738 cm^{-1} is ascribed to surface silanol groups.[24] It is clear that the intensity of this band is significantly reduced in the grafted material. This can be explained by the coordination of potassium cations to deprotanated silanol groups, which reduces the number of surface silanols. This confirms that K-grafted siloxy sites are created in the grafted USY catalyst.

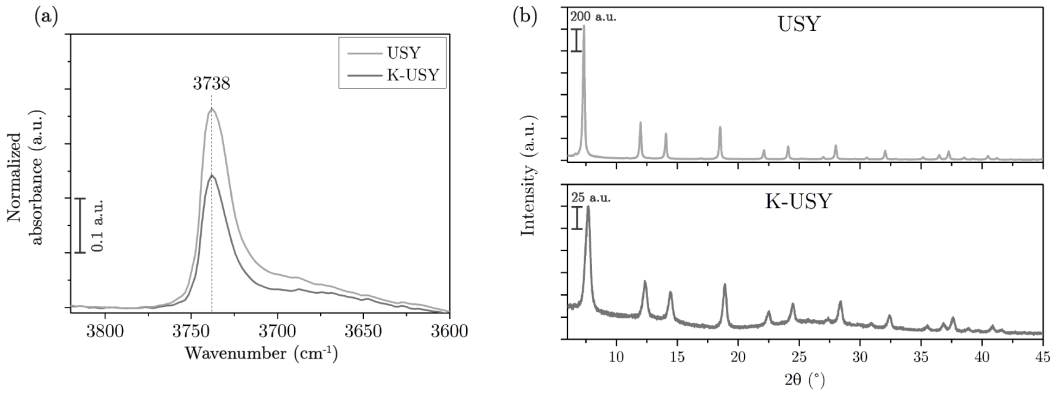

Figure 3.2: (a) Normalized IR absorbance spectrum of activated USY and K-USY in the region between 3820 and 3600 cm^{-1}. (b) XRD patterns of USY and K-USY in the region between 6 and 45 $2\theta°$.

The K-grafting procedure also has an impact on the structure of the USY zeolite. Using XRD measurements a decrease in crystallinity with regard to the parent USY zeolite is observed in K-grafted USY, as seen in Figure 3.2b. While contributions of the USY structure are predominant, amorphisation of the structure is observed by the broad humps between 5 and 15 $2\theta°$ and between 20 and 35 $2\theta°$. It is calculated by Keller et al. that the crystallinity is retained by 72 % compared to the parent USY. The reduction in crystallinity is accompanied by a 15% reduction in surface area and a 10% reduction in micropore volume, as is calculated using N_2 physisorption.[19] These observations illustrate that the zeolite pore structure has slightly degraded due to the K-grafting procedure. As the zeolite framework is an important factor for catalytic performance, this could influence the final catalytic performance of the K-grafted USY zeolite.

All together, it is observed that potassium is successfully incorporated in the USY catalyst by coordinating to deprotonated silanol groups. This incorporation has a small impact on the zeolite framework, which degraded slightly.

3.1.2 Active sites

In section 1.3 it was explained that the K-grafting procedure is expected to create basic sites of intermediate strength (O^{2-}-vacancies) and weak Lewis acid sites (K^+). Therefore, this section aims to clarify the changes in the basicity and acidity of the catalyst upon K-grafting.

Basicity

The nature of the basic sites present in the catalyst before and after K-grafting is studied by CO_2-IR. This technique is based on the interaction of the mildly acidic CO_2 molecule with basic sites present on the surface of the catalyst. During this interaction, different carbonates ($CO_3{}^{2-}$) form that absorb IR radiation between 1800 and 1300 cm^{-1}. The specific wavenumber at which the carbonate adsorbs radiation depends on the nature of the basic site that CO_2 interacts with.[25,41] Further details regarding CO_2-IR can be found in Appendix A. Generally, a free carbonate gives an absorbance band at 1415 cm^{-1}. This band splits if the carbonate is adsorbed on a surface, i.e.

when CO_2 interacts with a surface basic site. The splitting increment, $\Delta\nu_3$, is proportional to the strength of the surface basic site, as it is a measure of the interaction between the surface and the carbonate.

Figure 3.3 shows the IR absorbance spectra of the non-grafted USY (3.3a) and grafted K-USY (3.3b) catalysts in the region of interest with increasing CO_2 pressure. The formation of carbonates is not observed on the surface of USY, even when bands ascribed to gas phase CO_2 are observed around 2350 cm^{-1} (inset). This confirms the lack of basicity expected for the USY zeolite. In contrast, in the absorbance spectra of K-USY multiple bands between 1800 and 1300 cm^{-1} arise with increasing CO_2 pressure. As $\Delta\nu_3$ is between 226 cm^{-1} and 375 cm^{-1}, the bands are assigned to the formation of bidentate carbonate species. Since bidentate carbonate species form upon interaction of CO_2 with basic sites of moderate strength,[41] this confirms that upon K-grafting mildly basic sites are formed.

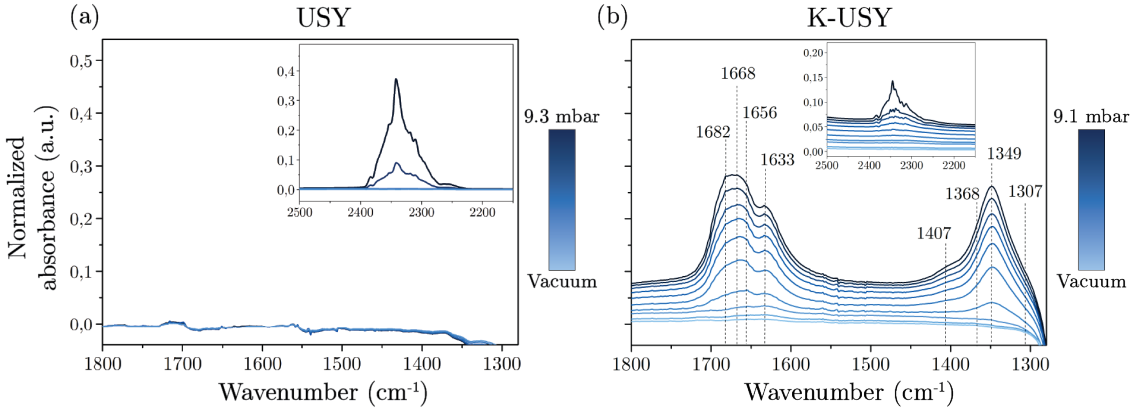

Figure 3.3: Normalized FT-IR spectra of the catalyst materials (a) USY and (b) K-USY during CO_2 adsorption at room temperature from vacuum conditions to ca. 9 mbar.

Acidity

The nature of the acid sites present in the catalyst before and after K-grafting is studied by pyridine-IR. This technique is based on the interaction of the basic pyridine molecule with both Brønsted and Lewis acid sites present on the surface of the catalyst. Depending on the type of site pyridine interacts with, different Py-complexes form that absorb IR radiation at characteristic energies. More detailed information on Py-IR can be found in Appendix A. In general, Lewis and relatively strong Brønsted acid sites can be easily distinguished as the formed pyridine species show bands in different regions. The pyridinium ion (PyH^+) absorbs IR radiation around 1540-1550 cm^{-1} and 1640 cm^{-1}, whereas coordinatively bound pyridine on Lewis acid sites (PyL) absorbs around 1440-1460 cm^{-1} and 1600-1635 cm^{-1}. Additionally, because hydrogen-bonded pyridine (H-bonded Py) is only observed at low evacuation temperatures below 150 °C, thermodesorption experiments enable the distinction between PyL and H-bonded Py.[42,43]

Figure 3.4 shows the IR absorbance spectra of the non-grafted USY (3.4a) and grafted K-USY (3.4b) catalysts in the region between 1650 and 1550 cm^{-1} obtained during a pyridine thermodesorption experiment. In none of the measured spectra contributions arising from PyH^+ are observed, indicating that neither USY nor K-USY contain Brønsted acid sites. Additionally, it can be seen that at 150 °C pyridine is no longer adsorbed on the USY surface, from which it can be concluded that only H-bonded pyridine had been adsorbed. This indicates that besides the absence of Brønsted acidity, USY does not contain Lewis acid sites. On the other hand, in the absorbance spectra obtained during pyridine thermodesorption on K-USY (Figure 3.4b) one clear band is still present at 150 °C. The band at 1590 cm^{-1} is attributed to a PyL-complex formed on a Lewis acid site created upon K-grafting, in which K^+ acts as a Lewis acid site. Further temperature increase to 200 °C results in the desorption of the LAS-coordinated pyridine from the surface, indicating that the Lewis acid site created during K-grafting has only weak acidic strength.

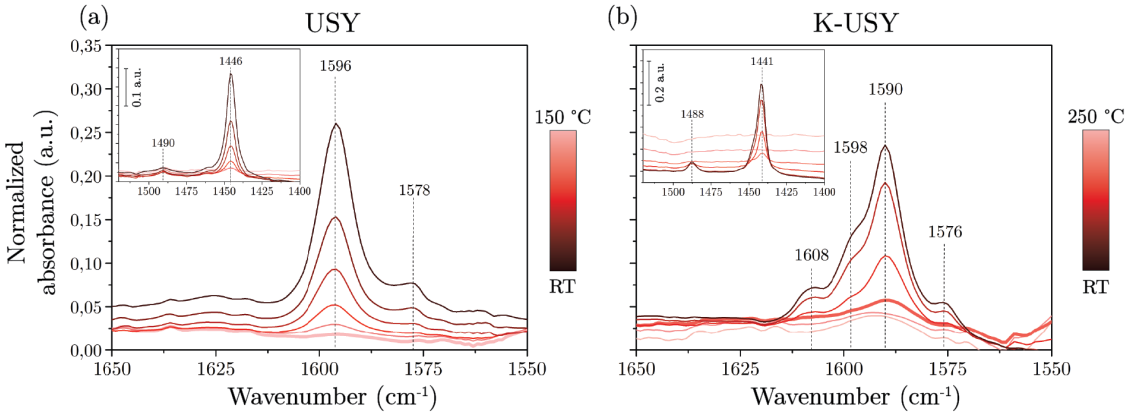

Figure 3.4: Normalized FT-IR spectra of the catalyst materials (a) USY and (b) K-USY during pyridine desorption from room temperature to 150 °C and 250 °C, respectively. The spectra taken at 150 °C are represented in bold.

To summarize, with CO_2- and Py-IR the changes in basicity and acidity upon K-grafting can be clearly identified. As a result of K-grafting, several active sites are created. Multiple basic sites of intermediate strength are created, as a consequence of stabilized oxygen vacancies formed during the K-grafting procedure. Additionally, the incorporation of K^+-cations results in the formation Lewis acid sites of weak acidic strength.

3.1.3 Catalytic performance

The aim of K-grafting USY is to increase the catalytic performance of the catalyst in the aldol condensation of propanal by the introduction of intermediate strength basic sites. In this section the changes in catalytic performance of the catalyst before and after K-grafting will be discussed. For this purpose, the aldol condensation of propanal is studied by *operando* measurements combined with on-line MS and *in-situ* measurements combined off-line GC using USY and K-grafted USY as catalysts. In Figure 3.5 the main results obtained from these measurements are summarized.

Activity Using GC it was calculated that the propanal conversion during one hour of reaction is significantly increased after K-grafting, by over 20 % compared to the parent USY, as shown in Figure 3.5a. The increased activity of the K-USY catalyst is confirmed by the IR spectra obtained during the first 20 minutes of the reaction. In the case of USY (Figure 3.5b) the absorption of propanal on the catalyst surface combined with the consumption of surface silanol groups is clearly observed ($\nu_{C=O}$, 1761 and 1744 cm^{-1}; ν_{O-H}, 3740 cm^{-1}). However, no IR bands ascribed to the products are seen. This is in contrast with the IR spectra obtained for the K-USY catalyst during the first 20 minutes of reaction (Figure 3.5c). For the K-USY catalyst, again the absorption of propanal on the surface accompanied by the consumption of silanol groups is observed ($\nu_{C=O}$, 1761 cm^{-1} and 1734 cm^{-1}; ν_{O-H}, 3740 cm^{-1}). However, additional IR bands ascribed to the aldol dimer ($\nu_{C=O}$, 1705 cm^{-1}) and even the aldol trimer ($\nu_{C=O}$, 1686 cm^{-1}) are observed as well. This illustrates that the increase in propanal conversion is accompanied by an increase in product formation.

Selectivity In *operando* experiments combined with on-line MS the product formation during reaction and desorption was followed over time. The obtained results are shown in Appendix B. The formation of the aldol condensation products and the main side product 3-pentanone (3P) could be observed. However, it was not possible to obtain a reliable quantitative and qualitative comparison of the catalyst selectivity based on MS. Therefore, *in-situ* experiments with off-line GC were used for more in-depth evaluation of the product distribution. With GC-MS analysis it was possible to identify the differences in product selectivity between the USY and K-USY catalysts, as is illustrated in Table 3.1. In both cases the desired aldol dimer product (2M2P) is identified. In the case of K-USY the observed product peak has a higher intensity, indicating that it is formed in a higher amount. The main undesired side product 3P, obtained via the Tishchenko reaction pathway (Scheme 1.3), was not observed when the reaction was catalyzed with K-USY, whereas

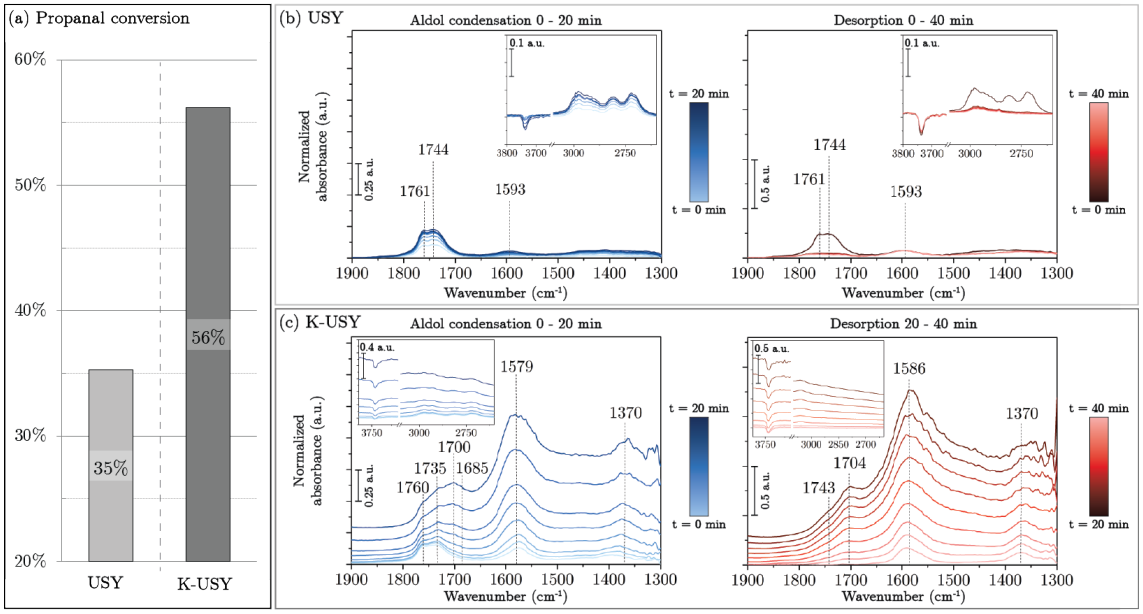

Figure 3.5: Overview of the main results obtained during the catalytic measurements using USY and K-USY as catalyst materials, showing (a) propanal conversion during one hour of reaction and (b),(c) normalized FT-IR absorbance spectra obtained during reaction and desorption.

Table 3.1: Summary of the results obtained from GC-MS analysis of the reaction mixtures from USY and K-USY.

Catalyst	2M2P presence	2M2P intensity[a]	3P presence	Additional products[b]
USY	Yes	1.36	Yes	3
K-USY	Yes	3.60	No	-

[a] Compared to the 2M2P peak intensity found for the blanc reaction
[b] Compared to the identified peaks for the K-USY catalyzed reaction

it was identified in the reaction using USY as catalyst. Moreover, three additional side products, solely oxygenated compounds, not observed for the reaction catalyzed by K-USY were identified for the reaction catalyzed by USY. These results indicate that the introduction of K-sites in USY leads to a higher selectivity towards the aldol condensation pathway rather then undesired reaction pathways. Unfortunately, it was not possible to quantify selectivity results by GC.

Deactivation In Figure 3.5 it is seen that the increased propanal conversion of K-grafted USY is accompanied by the formation of more aromatic species on the catalyst surface ($\nu_{C=C}$, 1593 cm^{-1} and 1590 cm^{-1};ν_{C-H}, 3050 cm^{-1}). Luckily, the aromatics desorb from the surface relatively easily once the reaction is stopped as indicated by the IR spectra obtained during the desorption. This is confirmed by the DRS-UV-VIS spectra obtained during reaction and desorption, shown in Appendix B. In these spectra the formation and subsequent desorption of polyaromatics ($\lambda > 500$ nm) is observed by an increase in baseline intensity, followed by a rapid decrease in intensity during desorption. The amount of coke still present in the K-USY catalyst after desorption was quantified by TGA-MS. This amounted to only 1.4 wt%. Since the aromatics forming on the catalyst surface desorb easily and the amount of coke that is present in K-USY after reaction is relatively small, it can be concluded that after K-grafting the catalyst remains stable against deactivation during the considered reaction time.

Long term stability It has been found that the K-grafted catalyst has a reduced long term stability caused by destabilization of the structure originating from the K-grafting process. Over time (> 1.5 years) loss in crystallinity, surface area and pore volume are observed as a result of

zeolite framework degradation. This has a significant impact on the catalytic performance of the catalyst, as *in-situ* measurements show that less products and more coke are formed during reaction. Hence, it is concluded that due to slow degradation the catalyst becomes less active and less stable against deactivation over time. The experimental data on which these results are based are summarized in Appendix B.

To conclude, from the *operando* and *in-situ* measurements performed during propanal aldol condensation reactions using USY and K-grafted USY as catalysts, it is found that the activity and selectivity of the catalyst significantly increase upon K-grafting. Additionally, the K-grafted catalyst remains stable against deactivation. The improvement in catalytic performance during the aldol condensation of propanal is related to the newly created mild basic and Lewis acid sites formed upon K-grafting. The small increase in catalyst deactivation can be explained by the increased activity towards C-C coupling resulting in increased coke formation. These observations confirm the results discussed by Keller et al.[19]

3.2 Attapulgite-bound technical catalyst

In this section the impact that upscaling with attapulgite clay has on the properties and performance of the technical catalyst will be discussed. Firstly, the changes in general material properties are analyzed using ICP-OES, SEM-EDX, XRD and Ar physisorption. Following, the nature of the basic and acid sites present in the catalyst after upscaling is elucidated. To conclude, the effects of upscaling from research to technical catalyst on the catalytic performance are discussed. Most of the measurements that will be discussed here are performed on the technical catalyst material in powder form, i.e. grinded. If a measurement is performed on the extrudate-shaped catalyst particle, this will be noted.

3.2.1 General characterization

During the upscaling process the research catalyst USY is firstly mixed and extruded with attapulgite clay, after which it is K-grafted. The incorporation of K is confirmed and quantified using ICP-OES. The K-grafted USY/Attapulgite extrudates contain 2.48 wt% K. Because attapulgite clay contains 0.58 wt% K, this means that 0.174 wt% K is obtained by mixing with the clay, while 2.31 wt% is incorporated by the K-grafting procedure. This is significantly less than the amount of K incorporated in the research catalyst (4.87 wt%). This can influence the amount of created active sites and thereby catalytic performance of the catalyst. In Figure 3.6 the distribution of the incorporated K in a shaped extrudate particle as determined with SEM-EDX is shown. It is observed that K is distributed everywhere in the extrudate. However, a weak gradient in K content can be observed starting on the edges and progressively moving in a radial direction towards the center. This indicates that the incorporation of K in the extrudate is diffusion limited, which might hinder the extent at which K is incorporated. Furthermore, the presence of areas in which K has accumulated is observed, which might originate from attapulgite regions in which K is already present.

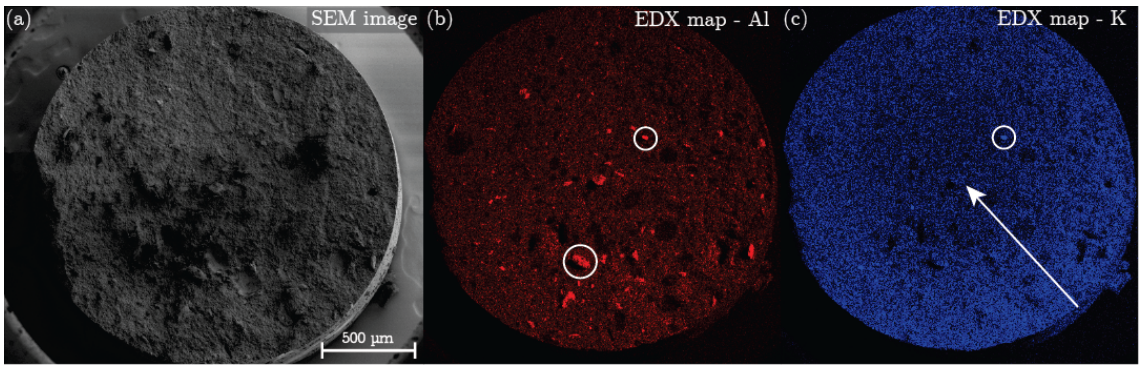

Figure 3.6: (a) SEM image of a K-(USY/Attapulgite) extrudate. (b),(c) EDX maps showing the distribution of Al (red) and K (blue) in the extrudate. The marked areas correspond to regions containing mainly clay, the arrow indicates the K-gradient.

Furthermore, the effect of upscaling on the crystallinity and pore accessibility was studied. With XRD measurements it is confirmed that the crystallographic structure has not degraded during the upscaling procedure. As is shown in Figure 3.7, contributions of the zeolite structure as well as the clay structure are present in the diffractogram of the technical K-(USY/Attapulgite) catalyst. No signs of amorphisation are observed. More information regarding the changes in pore structure during upscaling is obtained with Ar physisorption. An overview of the measured values is given in Table 3.2. Even tough the BET surface area is 13.8 % lower than the expected BET surface area according to the USY and clay mass percentages, the micropore volume is as high as 98 wt% of the expected value illustrating that the zeolite framework, from which the micropores originate, remains intact. This excellent stability of the zeolite structure is noteworthy, as this indicates that the incorporation of attapulgite stabilizes the USY phase against degradation during K-grafting.

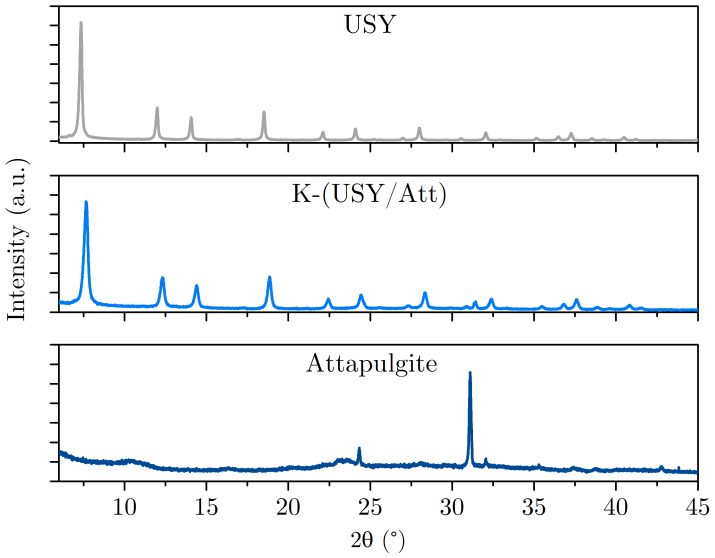

Figure 3.7: XRD patterns of USY, K-(USY/Attapulgite) and attapulgite in the region between 6 and 45 $2\theta^{\circ}$.

Table 3.2: Results from Ar physisorption analysis on USY, K-(USY/Attapulgite) and attapulgite.

Catalyst	S_{BET} (m^2 g^{-1})	V_{pore} (cm^3 g^{-1})	$V_{micropore}$ (cm^3 g^{-1})
USY	755.8	0.384	0.259
K-(USY/Att)	471.6	0.293	0.177
Attapulgite	60.3	0.156	-

From these results becomes clear that performing the proposed upscaling procedure with attapulgite as binder material technical K-grafted (USY/Attapulgite) extrudates are succesfully obtained. The upscaling process does not affect the zeolite framework and only a minor decrease in BET surface area is observed. During the K-grafting procedure K is successfully incorporated in technical catalyst, although the introduced amount was smaller compared to the research catalyst.

3.2.2 Active sites

In section 3.1 it has been shown that mild basic and Lewis acid sites are created upon K-grafting of the research catalyst. In this section the nature of the basic and acid sites obtained during the upscaling process of the technical K-grafted USY/Attapulgite catalyst will be discussed.

Basicity

The nature of the basic sites present in the technical catalyst and in the clay is studied with CO_2-IR. Figure 3.8 shows the IR absorbance spectra of the technical K-(USY/Attapulgite) catalyst and the attapulgite clay in the region between 1800 and 1300 cm^{-1} with increasing CO_2 pressure. It can be seen that on both the catalyst and the clay surface carbonates form upon interaction with CO_2.

In the case of attapulgite (Figure 3.8b), only one carbonate species has formed. As explained in Appendix B, the amount of splitting $\Delta\nu_3$ (209 cm^{-1}) indicates that this carbonate species is a bidentate carbonate, which illustrates that one type of basic site of intermediate strength is present in the clay. In the absorbance spectra of the technical catalyst multiple carbonate bands between 1800 and 1300 cm^{-1} arise with increasing CO_2 pressure. As these bands have a $\Delta\nu_3$ between 228 and 392 cm^{-1}, they are attributed to the formation of multiple bidentate carbonate species due to the interaction of CO_2 with several basic sites of intermediate strength present in the material. The presence of these basic sites cannot be solely attributed to the basic site obtained from incorporation of the clay (1631 cm^{-1}), indicating that basic sites are created during the K-grafting procedure applied on USY/Attapulgite. The basic sites generated in K-grafted USY/Attapulgite seem similar to those present in K-grafted USY, as they give rise to similar carbonate species upon interaction with CO_2.

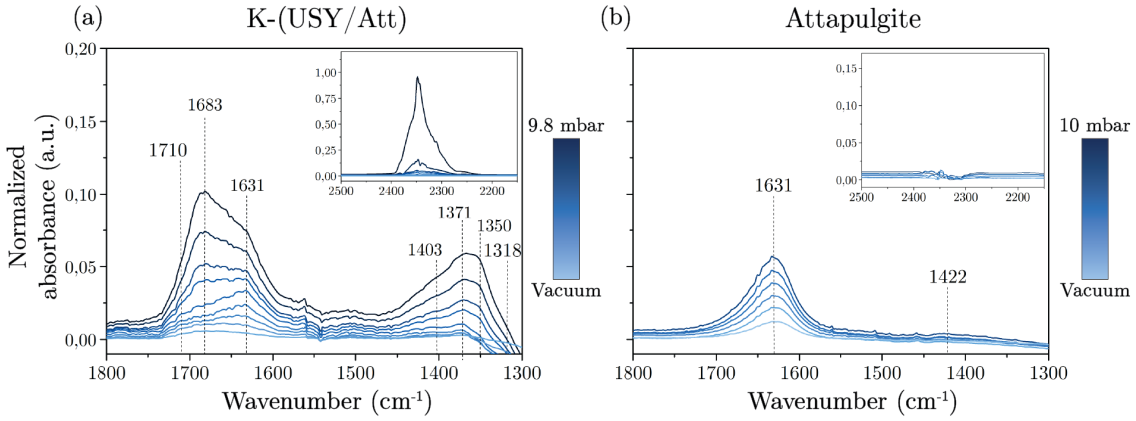

Figure 3.8: Normalized FT-IR spectra of the catalyst materials (a) K-(USY/Attapulgite) and (b) attapulgite during CO_2 adsorption at room temperature.

Even though bidentate carbonate absorbance bands corresponding to similar basic sites are observed in the CO_2-IR experiments performed on both K-USY and K-(USY/Attapulgite), the intensities of these bands differ significantly between the measurements. It is observed that the band intensity is much lower in the spectra obtained for the technical catalyst compared to the intensity measured for the research catalyst. This suggests that less basic sites are formed in the technical catalyst.

With CO_2-TPD the concentration of basic sites present in K-USY, K-(USY/Attapulgite) and attapulgite was determined. The results, shown in Table 3.3, confirm that indeed less basic sites are incorporated in the latter. This can be explained by two effects. Firstly, the amount of USY is diluted in this catalyst, as only 70% of the material consists of the zeolite. Because K is introduced in the catalyst after extrusion with attapulgite, it is not only incorporated into the zeolite, but also in the clay. Hence, the K^+-cations are used less efficiently to create basic sites. Yet, this does not explain the large decline in basicity, which is mainly due to the low incorporation of K. Because significantly less K is incorporated upon K-grafting in USY/Attapulgite compared to USY, less basic sites are created.

Acidity

The nature of the acid sites present in the attapulgite-bound technical catalyst and attapulgite clay has been studied by Py-IR. In Figure 3.9 the IR absorbance spectra obtained during pyridine thermodesorption experiments of the technical catalyst and the clay are shown in the region between 1650 and 1550 cm^{-1}.

Table 3.3: CO_2−TPD results from K-USY, K-(USY/Attapulgite) and attapulgite.

Catalyst	Adsorbed CO_2 (mL g^{-1})	Basic sites (mmol g^{-1})	T_{max} (°C)
K-USY	9.84	$4.39 \cdot 10^{-1}$	153
K-(USY/Att)	5.46	$2.44 \cdot 10^{-1}$	184
Attapulgite	6.59	$2.94 \cdot 10^{-1}$	223

Bands arising from the formation of PyH^+ were observed in neither of the experiments. This indicates that neither attapulgite clay, nor K-grafted USY/Attapulgite contain any Brønsted acid sites. In contrast, bands ascribed to pyridine coordinated to Lewis acid sites are seen in the spectra obtained for both materials. In the Py-IR spectrum of K-(USY/Attapulgite) at 150 °C two clear bands are observed. These arise from PyL instead of H-bonded Py. The band at 1590 cm^{-1} is attributed to PyL coordinated to the Lewis acid sites created upon K-grafting as it was previously observed for the K-grafted USY catalyst in section 3.1.

Additionally, a band arising at 1608 cm^{-1} is observed. Interestingly, this band is also present in the Py-IR spectra of attapulgite. Because the band remains present during temperature increase up to 350 °C, it results from pyridine adsorbed on strong Lewis acid sites. Therefore, the newly observed peak in the Py-IR experiment of K-(USY/Attapulgite) arises from strong Lewis acid sites due to the incorporation of attapulgite in the technical catalyst.

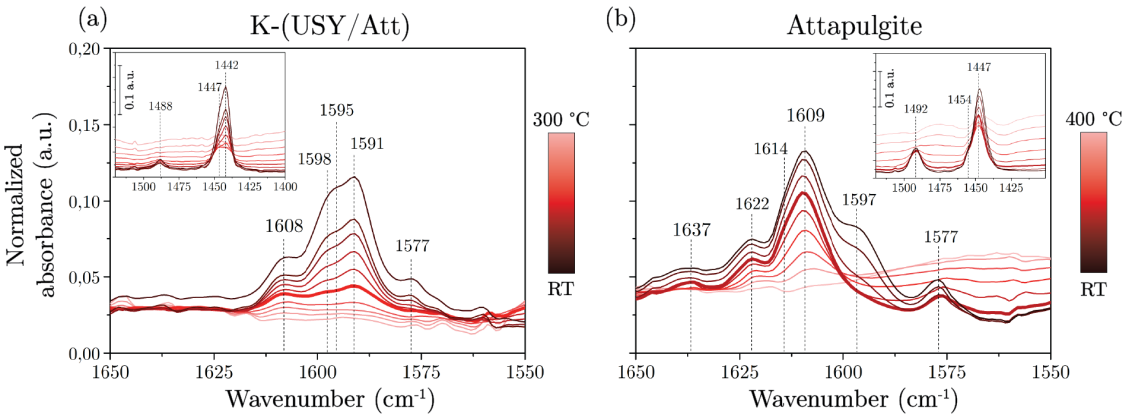

Figure 3.9: Normalized FT-IR spectra of the catalyst materials (a) K-(USY/Attapulgite) and (b) attapulgite during pyridine desorption from room temperature to 300 °C and 400 °C, respectively. The spectra taken at 150 °C are represented in bold.

The distribution of Lewis acid sites present in the shaped catalyst particles was visualized by CFM. For this purpose the extrudate was stained with a solution that reacts to form the fluorescent probe fluorescein. This reaction can be catalyzed by any type of acid sites. More information can be found in Appendix A. Since in the catalyst no Brønsted acid sites are present, in this way only Lewis acid sites will be visualized. As seen in Figure 3.10 the Lewis acid sites are distributed heterogenously within the extrudate. There are areas in which little fluorescence is seen (4), areas in which the fluorescence is more intense (3) and a gradient in intensity is observed from the edge of the extrudate inward ((1) and (2)). The presence of intenser fluorescence can be correlated with the incorporation of clay and K^+ in the catalyst by comparison of Figure 3.10 with Figure 3.6. It is seen that the areas with little fluorescence correspond to pores, while more intense areas correlate with areas containing predominantly clay as these introduce additional Lewis acid sites in the extrudate. Furthermore, the intensity gradient can be attributed to the introduction of K^+-sites in the catalyst upon K-grafting. This confirms that upon upscaling Lewis acid sites are introduced by the incorporation of attapulgite and by K-grafting. An alternative explanation for the intensity gradient can be the slow diffusion and accumulation of the reactants on the edge of the catalyst. However, further investigation is required to confirm this hypothesis.

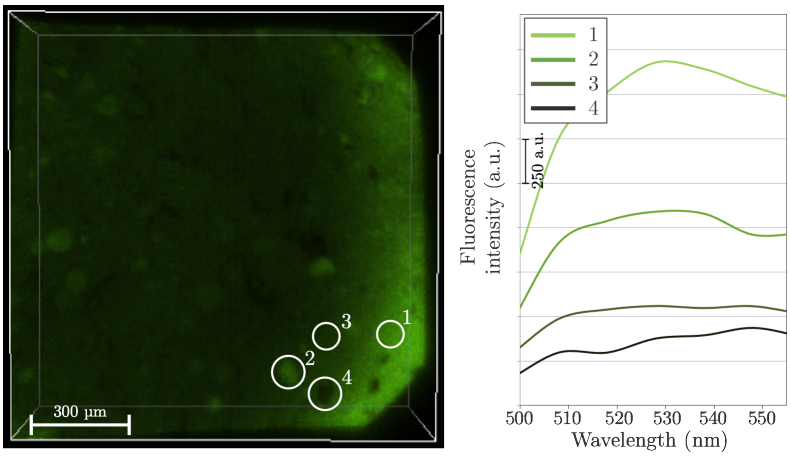

Figure 3.10: Confocal fluorescence microscopy image and spectral information obtained from the cross section of a K-(USY/Attapulgite) extrudate during the *in-situ* synthesis of fluorescein at 200 °C. λ_{ex} = 488 nm, detection 500–560 nm.

To conclude, with CO_2- and Py-IR and CFM analysis a comparison between the basicity and acidity of the K-grafted USY research catalyst and the K-grafted USY/Attapulgite technical catalyst can be made. During the upscaling process, several active sites are created. Similarly to the research catalyst, basic and Lewis acid sites of intermediate strength are incorporated in the technical catalyst via the K-grafting procedure. However, less of these active sites are created in the attapulgite-bound technical catalyst, as less K is incorporated than in the K-grafted USY powder. Furthermore, the incorporation of attapulgite results in the inclusion of additional mildly basic sites and strong Lewis acid sites in the technical catalyst.

3.2.3 Catalytic performance

It is crucial controlling that the upscaling process does not have a (large) detrimental influence on the catalytic performance of the technical catalyst compared to the performance of the research catalyst. In this section the effect of upscaling on the catalytic performance of the technical K-(USY/Attapulgite) catalyst will be discussed. Firstly, this is discussed for the case that the catalyst is grinded and pressed into a wafer, which will subsequently be compared with the extrudate-shaped catalyst particle. Finally, the changes in catalytic performance will be connected to the altered catalyst properties reviewed in the previous sections.

In Figure 3.11 the main results from the catalytic measurements on K-grafted USY/Attapulgite and attapulgite are summarized. In these catalytic measurements the aldol condensation of propanal over these materials was studied by *operando* and *in-situ* measurements with on-line MS and off-line GC, respectively.

Activity Using GC analysis it was found that the propanal conversion during one hour of reaction over the technical catalyst is reduced by 8 % compared to the research catalyst, from 56 % to 48 %. This reduction in activity is confirmed by *in-situ* IR data, as shown in Figure 3.11b. The band ascribed to the formation of dimer ($\nu_{C=O}$, 1700 cm^{-1}) during the first 30 minutes of reaction is less pronounced than for the dimer band observed with the research catalyst (Figure 3.5c). Additionally, no band attributed to trimer product is observed. The drop in conversion cannot be explained by mixing of the zeolite with clay, as a slightly higher conversion is obtained for attapulgite. However, the decrease in active sites discussed in the previous section can explain both the reduced conversion and the reduced product formation. In section 3.1 it was demonstrated that K-grafting induced a higher propanal conversion and a higher selectivity towards aldol dimer and trimer products. Therefore the lower activity of the technical catalyst might be connected to the lower K^+-content rather than the incorporation of attapulgite.

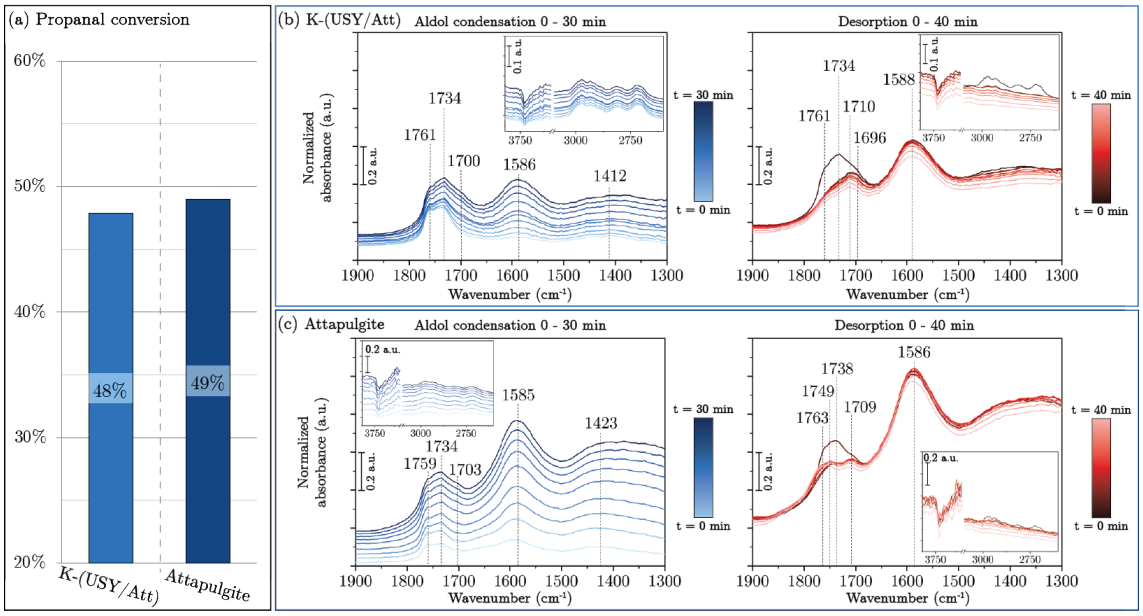

Figure 3.11: Overview of the main results obtained during the catalytic measurements using K-(USY/Attapulgite) and attapulgite as catalyst materials, showing (a) propanal conversion during one hour of reaction and (b),(c) normalized FT-IR absorbance spectra obtained during reaction and desorption.

Selectivity Given the difficulty in determination of the selectivity with *in-situ* FT-IR and on-line MS analysis (Figure 3.11b, B.2 and B.4), the changes in selectivity were mainly derived from GC-MS analysis. The former techniques indicated a reduction in selectivity upon upscaling, because the formation of aldol products was not clearly observed with FT-IR and on-line MS suggested the formation of more undesired side products, i.e. 3-pentanone and propyl propionate. This is in line with the results obtained with GC-MS (Table 3.4), which showed that the selectivity of the attapulgite-bound technical catalyst is slightly reduced upon upscaling. Of the expected products, the desired aldol dimer product (2M2P), is clearly observed, whereas the undesired side product, 3-pentanone (3P), could not be detected. Additionally, only one side product not observed in the reaction using K-USY as catalyst was identified. This high selectivity towards the aldol condensation pathway is solely attributed to the incorporation of K^+-cations in the technical catalyst, as attapulgite did not show good selectivity. The reaction products identified in the reaction catalyzed by attapulgite, include the desired dimer product, the undesired side product 3-pentanone, as well as six additional side products not observed for the reaction catalyzed by K-USY were identified. The additional side products included both oxygenated and non-oxygenated species. Unfortunately, it was not possible to quantify the selectivity results by GC.

Table 3.4: Summary of the results obtained from GC-MS analysis of the reaction mixtures from K-(USY/Attapulgite) and attapulgite.

Catalyst	2M2P presence	2M2P intensity[a]	3P presence	Additional products[b]
K-(USY/Att)	Yes	2.48	No	1
Attapulgite	Yes	2.80	Yes	6

[a] Compared to the 2M2P peak intensity found for the blanc reaction
[b] Compared to the identified peaks for the K-USY catalyzed reaction

Deactivation Besides the decrease in propanal conversion and the slight reduction in selectivity, the upscaling process also has an impact on the deactivation of the technical catalyst. This can be readily observed in the IR spectra obtained during the 40 minutes of desorption after the reaction over K-(USY/Attapulgite) shown in Figure 3.11b. It is seen that the aromatic species ($\nu_{C=C}$, 1588

cm^{-1}) formed on the surface desorb very slowly once the reaction is stopped. This effect is even more pronounced in case of attapulgite, where the aromatics ($\nu_{C=C}$, 1586 cm^{-1}) do not easily desorb as well. These results are confirmed by the DRS-UV-VIS spectra obtained during reaction and desorption, as shown in Appendix B. In the spectra obtained for both K-(USY/Attapulgite) and attapulgite the formation of polyaromatics is observed by an increase in baseline intensity. During desorption only a small decrease in intensity is observed.

The amount of coke present in the spent technical catalyst and in the spent clay after 40 minutes of desorption was quantified using TGA-MS. The results are shown in Table 3.5. It was found that in the technical catalyst more coke formed compared to the research catalyst, 4.5 wt% in case of a wafer-shaped spent catalyst and 3.0 wt% in case of an extrudate-shaped spent catalyst. However, the deactivation is not as severe as for the clay, which contained 6.7 wt% coke. Furthermore, the higher combustion temperature at which coke is burned off in attapulgite indicates that the coke is of a harder nature (i.e. higher C/H ratio).[44] These results indicate that the inclusion of attapulgite induces more coke formation in the technical catalyst. This was studied more in-depth with CFM by visualizing the areas in which polyaromatics had formed on the spent K-(USY/Attapulgite) extrudate.

Table 3.5: Results from TGA-MS analysis on K-USY, K-(USY/Attapulgite) and attapulgite spent samples.

Catalyst	Weight loss (wt%)	$T_{combustion}$ (°C)
K-USY	1.4	-
K-(USY/Att) wafer	4.5	490
K-(USY/Att) extrudate	3.0	443
Attapulgite	6.7	499

In Figure 3.12 the CFM image obtained for a spent K-grafted USY/Attapulgite extrudate is shown. It is seen that the fluorescent polyaromatics are distributed throughout the extrudate in a heterogeneous manner. Areas with more intense fluorescence are observed, whose emission spectra show that these areas are about twice as intense as the average intensity. Coke species similar in nature are present everywhere in the extrudate, as the emission spectrum only differs in intensity not in profile. This illustrates that the inclusion of attapulgite in the catalyst induces catalyst deactivation due to coke formation. This effect can be explained by the presence of strong Lewis acid sites in attapulgite. Due to a stronger interaction with these active sites, reactants are less likely to desorb from the catalyst. Instead, they remain on the catalyst surface and react further to form coke, subsequently deactivating the catalyst.

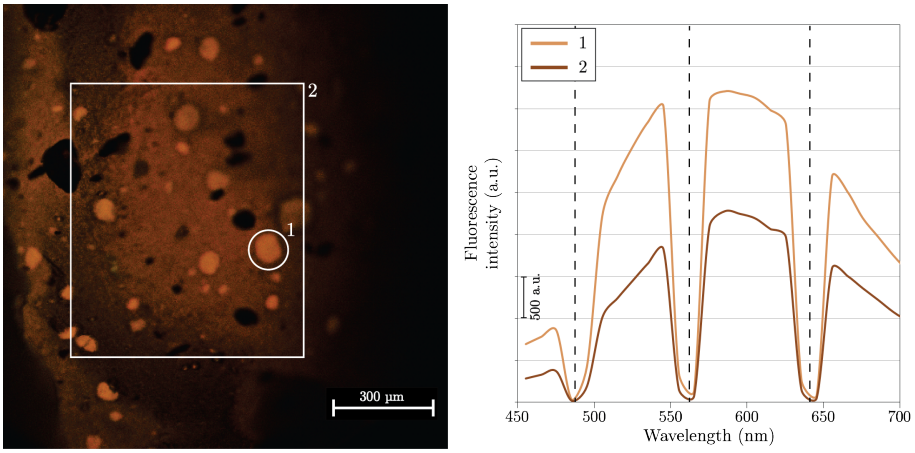

Figure 3.12: Confocal fluorescence microscopy image and spectral information obtained from the cross section of a spent K-(USY/Attapulgite) extrudate. λ_{ex} = 404, 488, 561 and 642 nm, detection 450–700 nm. The dashed lines indicate the excitation lasers.

Shaping effects As previously seen by the differences in coke present in the spent K-grafted (USY/Attapulgite) extrudate compared to the spent K-(USY/Attapulgite) wafer, the shape of the technical catalyst used in the aldol condensation reaction can impact the catalytic performance of the catalyst. In case of K-grafted USY/Attapulgite extrudates the conversion is increased by over 10 % compared to the sample pressed to a wafer. Additionally, the stability of the catalyst is slightly increased, as 1.5 wt% less coke is formed in the spent extrudate compared to the wafer. All together this shows that the shape of the technical catalyst has a significant impact on the performance. The differences in activity and stability can be explained by a reduction in catalyst deactivation. This results in a catalyst that remains active for longer time-on-stream, thereby increasing propanal conversion. To uncover the origin of the reduced deactivation further investigation is required.

Overall, it is clear that the upscaling process has a large impact on the final catalytic performance of the catalyst. This impact is attributed to both K-grafting of the technical catalyst and the incorporation of attapulgite. Firstly, the decrease in propanal conversion and aldol product formation can be attributed to the decrease in incorporated active sites. On the other hand, the high selective character of the catalyst still originates from the introduction of K^+-ions, even if less cations are incorporated. Furthermore, the increase in catalyst deactivation is caused by the strong Lewis acid sites arising from the clay inclusion.

3.3 Bentonite-bound technical catalysts

In this section the effect that the upscaling procedure has on the technical catalyst, when bentonite clay is used as binder, will be discussed. Firstly, the changes in the general material properties are reviewed using ICP-OES, SEM-EDX, IR spectroscopy, XRD and Ar physisorption. Subsequently, the nature and amount of the basic and acid sites that are created during the upscaling process are analyzed with CO_2-IR, CO_2-TPD and Py-IR. Finally, the catalytic performance of the non-grafted and K-grafted technical catalyst will be discussed and correlated with the previous results. Most of the measurements explained here are performed on the technical catalyst material in powder form, i.e. grinded. If a measurement is performed on the extrudate-shaped catalyst, this will be stated clearly.

3.3.1 General characterization

During the upscaling process the research catalyst USY is firstly mixed and extruded with bentonite clay, after which it is grafted with potassium. The incorporation of K is confirmed and quantified using ICP-OES. The K-grafted USY/Bentonite extrudates contain 0.85 wt% K. Before grafting 0.13 wt% K is already present in the USY/Bentonite extrudates, introduced by mixing with bentonite, which contains 0.45 wt% K. From this it is derived that only 0.72 wt% K is incorporated in the technical catalyst as a result of the K-grafting procedure. This is less than the amount of K incorporated in the research catalyst (4.87 wt%) and even in the attapulgite-bound technical catalyst (2.30 wt%). The distribution of the incorporated K in a shaped extrudate was determined with SEM-EDX. As seen in Figure 3.13, K is distributed everywhere throughout the extrudate. A weak gradient in K content starting on the edges and progressively moving in a radial direction towards the center is observed. This shows that the incorporation of K is diffusion limited. Additionally, areas where K has accumulated are seen. These agglomerates might arise from bentonite, as an increased amount of Al provided by the clay is present in these areas as well.

Furthermore, Keller et al. found that during the grafting process the potassium cations graft to deprotonated silanol groups (Figure 1.7).[28] This is analyzed in the case of the bentonite-bound technical catalysts with IR spectroscopy, as is shown in Figure 3.14. Here the IR absorbance in the OH-stretching region is shown for both the non-grafted USY and USY/Bentonite catalysts, as well as the grafted K-(USY/Bentonite) catalyst. In the spectrum of USY/Bentonite contributions of surface -OH groups from USY (ν_{O-H}, 3736 cm^{-1}) and bentonite (ν_{O-H}, 3640 cm^{-1}) are seen. The intensities of both bands decrease upon K-grafting. This indicates that potassium cations coordinate to both deprotanated silanol groups present in the active phase USY, as well as surface -OH groups present in the clay.

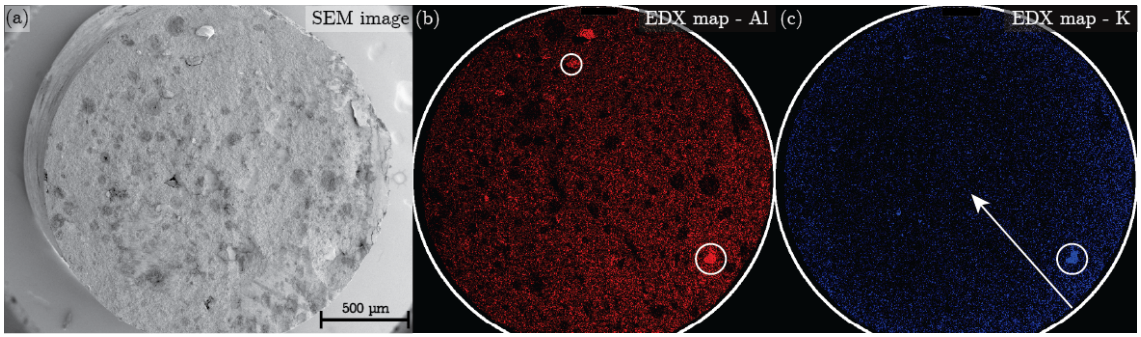

Figure 3.13: (a) SEM image of a K-(USY/Bentonite) extrudate. (b),(c) EDX maps showing the distribution of Al (red) and K (blue) in the extrudate. The marked areas correspond to regions containing mainly clay, the arrow indicates the K-gradient.

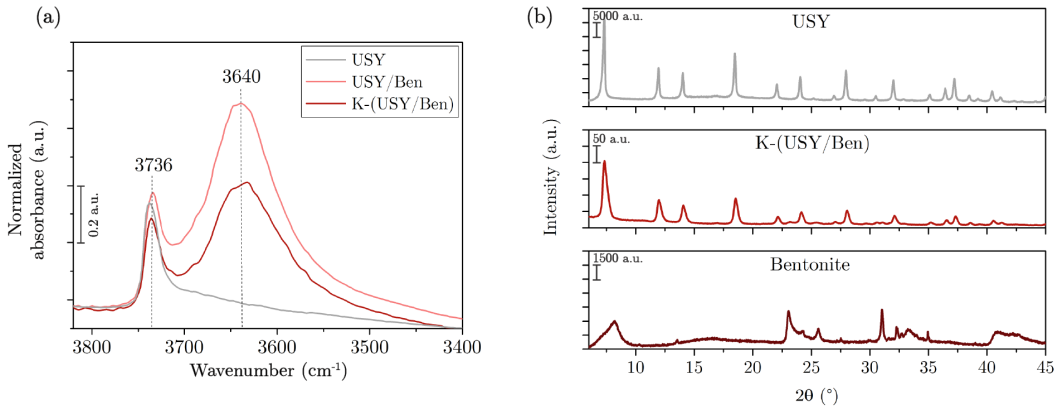

Figure 3.14: (a) Normalized IR absorbance spectrum of activated USY, USY/Bentonite and K-(USY/Bentonite) in the region between 3820 and 3400 cm^{-1}. (b) XRD patterns of USY, K-(USY/Bentonite) and bentonite in the region between 6 and 45 $2\theta°$.

With XRD measurements it is confirmed that the crystallographic structure has not significantly degraded during the upscaling process. In the diffractogram of the technical K-grafted bentonite-bound catalyst shown in Figure 3.14, contributions of both the zeolite structure and the clay structure are present. Even tough the lower intensity and broader width of the peaks indicate slight amorphisation, the crystallographic structure remains largely intact. The changes in pore structure during upscaling are further studied by Ar physisorption. The obtained information is summarized in Table 3.6. It can be seen that upon extrusion of USY with bentonite the surface area and micropore volume are as high as 91.2 and 93 % of the expected value, respectively, based on the USY:clay mass ratio. The total pore volume is even increased by 9 %. This is linked to the incorporation of bentonite, as it has been reported that this provides additional meso- and macroporosity within the technical catalyst.[37,39] Interestingly, upon K-grafting both the surface area and micropore volume of the material increase to 97.9 and 97.5 % of the expected values. This can be explained by dissolution of the material, thereby increasing the accessibility of the micropores within the structure upon grafting.

To sum up, it is seen that stable USY/Bentonite and K-grafted USY/Bentonite extrudates are obtained during the upscaling process with bentonite clay. The extrusion procedure has a small impact on the crystallographic structure and pore structure of the catalyst. The inclusion of bentonite provided additional porosity. In the subsequent K-grafting step a small amount of K (0.72 wt%) was successfully incorporated in the material. The incorporated K^+-cations coordinate to surface -OH groups present in USY and in bentonite. This can have a significant impact on the active sites present in the K-grafted USY/Bentonite catalyst.

Table 3.6: Results from Ar physisorption analysis on USY, USY/Bentonite, K-(USY/Bentonite) and bentonite.

Catalyst	S_{BET} (m^2 g^{-1})	V_{pore} (cm^3 g^{-1})	$V_{micropore}$ (cm^3 g^{-1})
USY	755.8	0.384	0.259
USY/Ben	489.8	0.312	0.170
K-(USY/Ben)	525.8	0.300	0.178
Bentonite	26.8	0.061	0.004

3.3.2 Active sites

In section 3.1 and 3.2 it has been shown that mild basic and Lewis acid sites are created upon K-grafting of the research USY and technical USY/Attapulgite catalysts. Additionally, it was found that active sites are introduced due to incorporation of attapulgite clay. In this section the nature and amount of the basic and acid sites obtained during the upscaling process of the bentonite-bound technical catalysts will be analyzed.

Basicity

The nature of the basic sites present in the non-grafted and grafted bentonite-bound technical catalysts is studied with CO_2-IR. In Figure 3.15 the IR absorbance spectra of both materials in the region between 1800 and 1300 cm^{-1} with increasing CO_2 pressure is shown. It can be seen that the obtained spectra for both catalysts look very similar. Upon interaction of CO_2 with the materials one low intensity band (1628 and 1633 cm^{-1}) is formed. This band is ascribed to the formation of a bidentate carbonate species on basic sites of intermediate strength. As a similar band (1628 cm^{-1}) is observed in the CO_2-IR spectra of bentonite (Figure B.9), this carbonate band is attributed to sites originating from the incorporation of bentonite in the technical catalysts. From the intensity of the bands it can be concluded that only a small amount of the incorporated basic sites is present in USY/Bentonite and K-grafted USY/Bentonite.

In the previous sections it was shown that upon K-grafting additional basic sites of weak moderate strength can be created. Interaction of CO_2 with these sites results in the formation of bidentate carbonates observed in the region between 1682 and 1633 cm^{-1}. However, as seen in Figure 3.15b, no additional carbonates form on the surface of K-grafted USY/Bentonite. Hence, no additional basic sites have been formed during the K-grafting process.

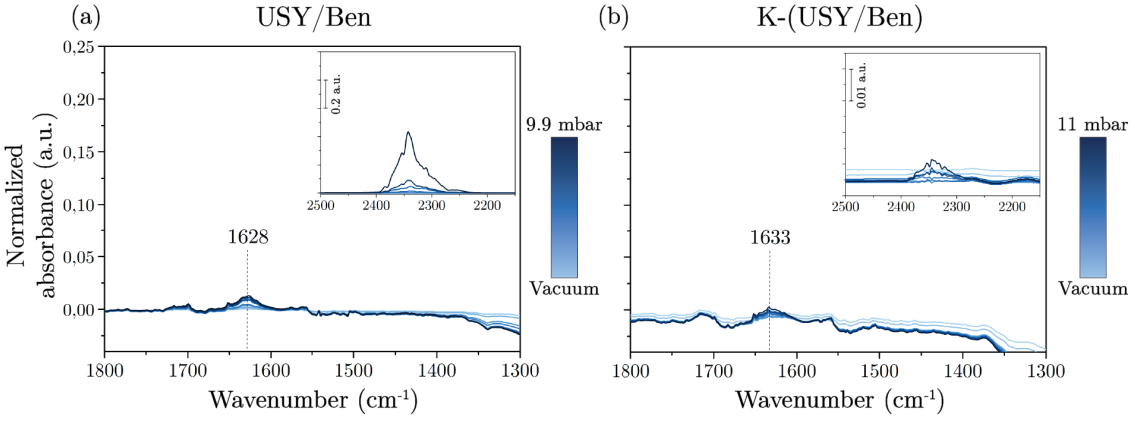

Figure 3.15: Normalized FT-IR spectra of the catalyst materials (a) USY/Bentonite and (b) K-(USY/Bentonite) during CO_2 adsorption at room temperature.

The amount of basic sites present in the bentonite-bound technical catalysts and bentonite clay was determined using CO_2-TPD. However, due to the low concentration of sites present in the materials very little CO_2 desorbed during the measurements, always less than 1 cm^3 g^{-1}. This causes a high uncertainty in the observed values, thereby hindering extensive quantitative analysis. This does illustrate that no observable amount of additional basic sites was incorporated in the

bentonite-bound technical catalyst upon K-grafting, which is in line with the CO_2-IR result that in the K-grafted USY/Bentonite catalyst no additional basic sites are formed.

Acidity

The amount and nature of the acid sites present in the bentonite-bound technical catalysts as well as bentonite clay have been studied by Py-IR. During both the agglomeration and extrusion of USY with bentonite and the post-synthetic K-grafting procedure interesting changes in the acidity of the obtained material are observed. Therefore, in the first part of this section the changes upon extrusion are discussed, after which the changes arising from the K-grafting procedure are reviewed.

In Figure 3.16 the IR absorbance spectra obtained during pyridine thermodesorption experiments of the non-grafted technical USY/Bentonite catalyst and the bentonite clay are shown in the region between 1650 and 1550 cm^{-1}. In the IR absorbance spectrum of bentonite taken at 150 °C bands ascribed to pyridine interacting with both Brønsted (1638 cm^{-1}) and Lewis (1621 and 1609 cm^{-1}) acid sites can be clearly observed. Upon temperature increase to 260 °C the PyH^+-band disappears, whereas the PyL-bands remain present even up to 300 °C. This indicates that Brønsted acid sites of intermediate strength and Lewis acid sites of high strength are present in bentonite clay. In the IR absorbance spectrum of USY/Bentonite taken at 150 °C the bands ascribed to these sites are clearly observed as well. Thus, acid sites originating from the clay are incorporated in the technical catalyst upon agglomeration and extrusion of USY with bentonite. Furthermore, in the spectrum of USY/Bentonite obtained at 150 °C a band at 1596 cm^{-1} is observed. Previously, this band was assigned to H-bonded pyridine arising from interaction with surface silanol groups on the USY surface (Figure 3.3). This interaction was very weak as pyridine was no longer adsorbed on the surface at 150 °C. It seems that the interaction between H-bonded pyridine and the USY surface silanols has become stronger upon extrusion with bentonite, as the H-bonded pyridine remains adsorbed until 200 °C. This indicates that interaction between USY and bentonite results in the formation of weak Brønsted acid sites.

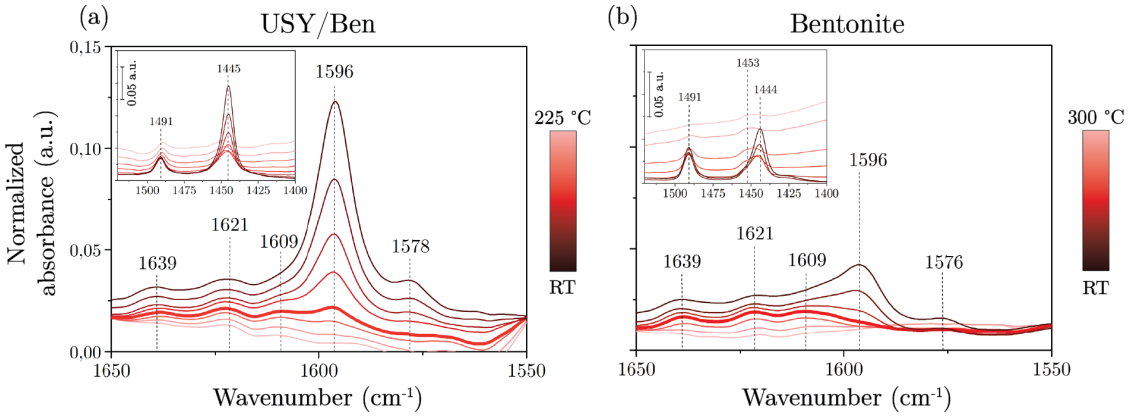

Figure 3.16: Normalized FT-IR spectra of the catalyst materials (a) USY/Bentonite and (b) bentonite during pyridine desorption from room temperature to 225 °C and 300 °C, respectively. The spectra taken at 150 °C are represented in bold.

The IR absorbance spectra obtained during pyridine thermodesorption experiments of the non-grafted USY/Bentonite and grafted K-(USY/Bentonite) catalysts in the region between 1650 and 1550 cm^{-1} are shown in Figure 3.17. It is expected that the K-grafting procedure incorporates additional Lewis acid sites in the K-grafted USY/Bentonite catalyst. In the research catalyst and attapulgite-bound technical catalyst, this was observed by the formation of a PyL band at 1590 cm^{-1}. However, no additional bands are observed in the Py-IR spectrum obtained at 150 °C in the case of K-grafted USY/Bentonite compared to non-grafted USY/Bentonite. This indicates that no sufficiently strong Lewis acid sites are created upon K-grafting of USY/Bentonite. Additionally, it seems that the bands attributed to PyH^+- and PyL-complexes (1639, 1623 and 1609 cm^{-1}) present in USY/Bentonite become less pronounced upon K-grafting. This indicates that instead of incorporating Lewis acid sites, K-grafting results in the removal of acid sites. Likely, because cation migration from the extrudate to the solution medium has occurred.

The amount of Brønsted and Lewis acid sites can be determined from the characteristic bands around 1545 and 1455 cm^{-1}, respectively.[45] As no pronounced band attributed to Brønsted acid sites is observed in the spectra obtained for USY/Bentonite and K-(USY/Bentonite) at 150 °C, only the amount of Lewis acid sites is determined. It is found that after the grafting procedure the number of sites has decreased by 41.6% from $1.10 \cdot 10^{-2}$ mmol acid sites g^{-1} to $0.64 \cdot 10^{-2}$ mmol acid sites g^{-1}. This confirms that during the K-grafting procedure Lewis acid sites are removed from the bentonite-bound catalyst.

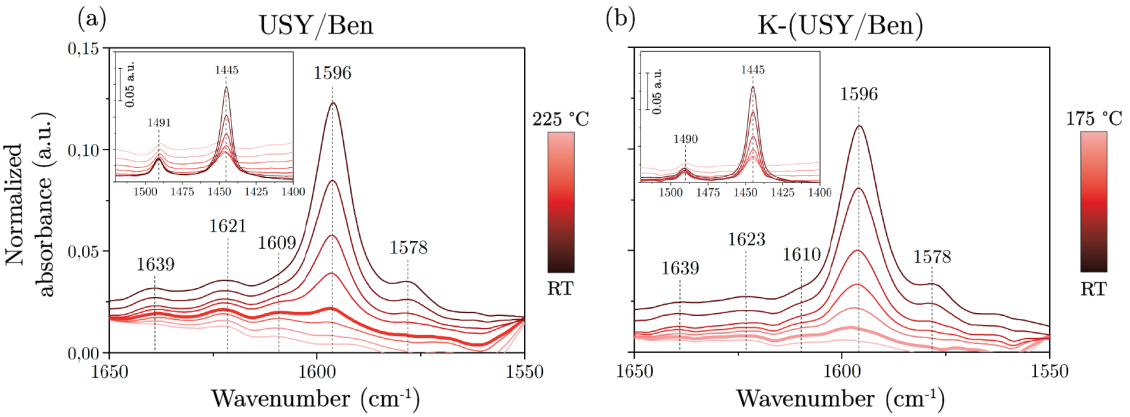

Figure 3.17: Normalized FT-IR spectra of the catalyst materials (a) USY/Bentonite and (b) K-(USY/Bentonite) during pyridine desorption from room temperature to 225 °C and 175 °C, respectively. The spectra taken at 150 °C are represented in bold.

The distribution of acid sites present in both USY/Bentonite and K-grafted USY/Bentonite was visualized by CFM. For this purpose fluorescein was used as probe molecule. Because the fluorescein staining reaction is catalyzed by any type of acid site, both Lewis and Brønsted acid sites present in the extrudates can be visualized. The CFM images obtained after staining are shown in Figure 3.18. When comparing the fluorescence distribution in the technical catalysts before and after K-grafting, it becomes clear that similar distributions are found. Areas with little fluorescence and more intense fluorescence are observed, corresponding to pores and bentonite-containing areas, respectively. It was expected that after K-grafting less fluorescence would be observed near the edge of the extrudate, as Py-IR indicated that Lewis acid sites are removed from the extrudate. However, due to the low intensity of the fluorescence, this is not clearly seen.

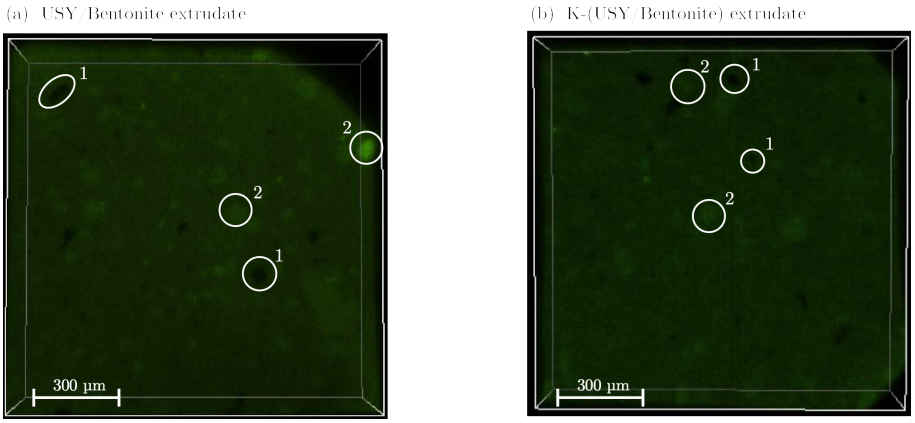

Figure 3.18: Confocal fluorescence microscopy images obtained from the cross section of a (a) USY/Bentonite and (b) K-(USY/Bentonite) extrudate during the *in-situ* synthesis of fluorescein at 200 °C. λ_{ex} = 488 nm, detection 500–560 nm. The indicated areas represent (1) pores and (2) clay domains.

To summarize, with CO_2-IR and Py-IR the changes in basicity and acidity during the upscaling process have been identified. Upon agglomeration and extrusion of USY with bentonite, basic sites as well as Brønsted and Lewis acid sites present in the clay are introduced in the technical USY/Bentonite catalyst. The incorporation of K^+ in the catalyst due to the grafting procedure, does not introduce additional basic and Lewis acid sites. On the contrary, the amount of active sites present in the K-grafted USY/Bentonite catalyst is significantly reduced.

3.3.3 Catalytic performance

In the previous section it was shown that upscaling has a surprising effect on the active sites present in the bentonite-bound technical catalysts. As the catalytic performance largely depends on the active sites, this section focuses on the effect of upscaling on the catalytic performance of USY/Bentonite and K-grafted USY/Bentonite catalysts. For this purpose, the results obtained during *operando* and *in-situ* measurements, respectively combined with on-line MS and off-line GC of USY/Bentonite, K-(USY/Bentonite) and bentonite will be discussed. Figures 3.19 and 3.20 show the main results observed during these measurements.

Activity As can be observed in Figure 3.19a, the first step of the upscaling procedure, the agglomeration and extrusion of USY with bentonite, results in a technical catalyst with 47 % propanal conversion. Compared to the parent USY powder this is an increase of 12 %. This increase is attributed to the incorporation of bentonite, as a conversion of 53 % is observed in the reaction catalyzed by the clay. After the final step of the upscaling procedure, K-grafting of USY/Bentonite, the conversion is increased by 9 % to 56 %. Interestingly, the increase in propanal conversion is accompanied by only a minor increase in product formation ($\nu_{C=O}$, 1704 cm^{-1}) observed by *in-situ* IR (Figure 3.20b).

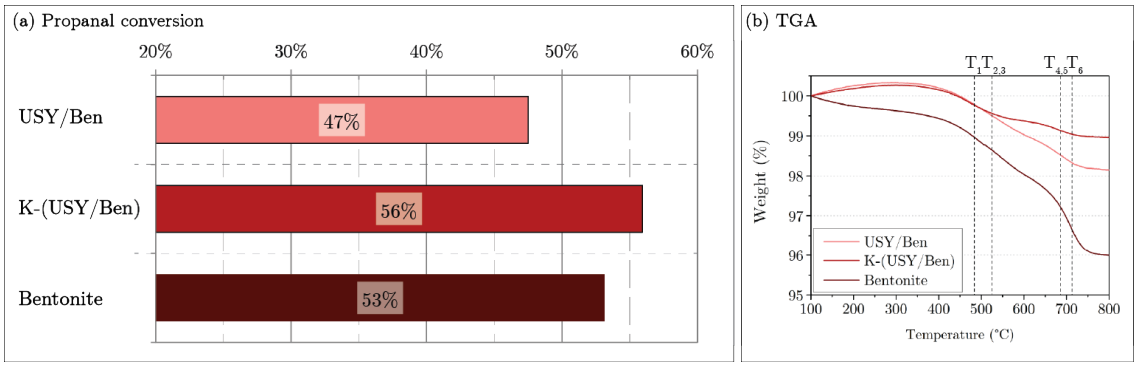

Figure 3.19: Comparison of (a) propanal conversion during one hour of reaction and (b) TGA of spent extrudates obtained for USY/Bentonite, K-(USY/Bentonite) and bentonite. The combustion temperatures of coke present in USY/Bentonite (T_2, T_5), K-(USY/Bentonite) (T_1, T_4) and bentonite (T_3, T_6) are indicated by the dashed lines.

Selectivity Interesting results are obtained regarding the selectivity of the bentonite-bound catalysts, before and after K-grafting. In the non-grafted USY/Bentonite catalyst, the formation of products is not clearly observed in the IR spectra obtained during reaction. However, when the desorption of propanal is started, instead of desorption of adsorbed species the formation of new species is observed (Figure 3.20a). New bands at 1830, 1779 and 1713 cm^{-1} appear, accompanied by the consumption of clay surface-OH groups. These bands are generally ascribed to $\nu_{C=O}$ vibrations of carboxylic acid anhydride, carboxylic acid and ester species.[46] These species may form via the Tishchenko reaction (Scheme 1.3). Interestingly, the formation of these species is only observed in the case of USY/Bentonite, not in the case of bentonite. This indicates that the interaction between USY and bentonite results in a technical catalyst that is not selective towards the aldol formation pathway, but towards the Tishchenko pathway.

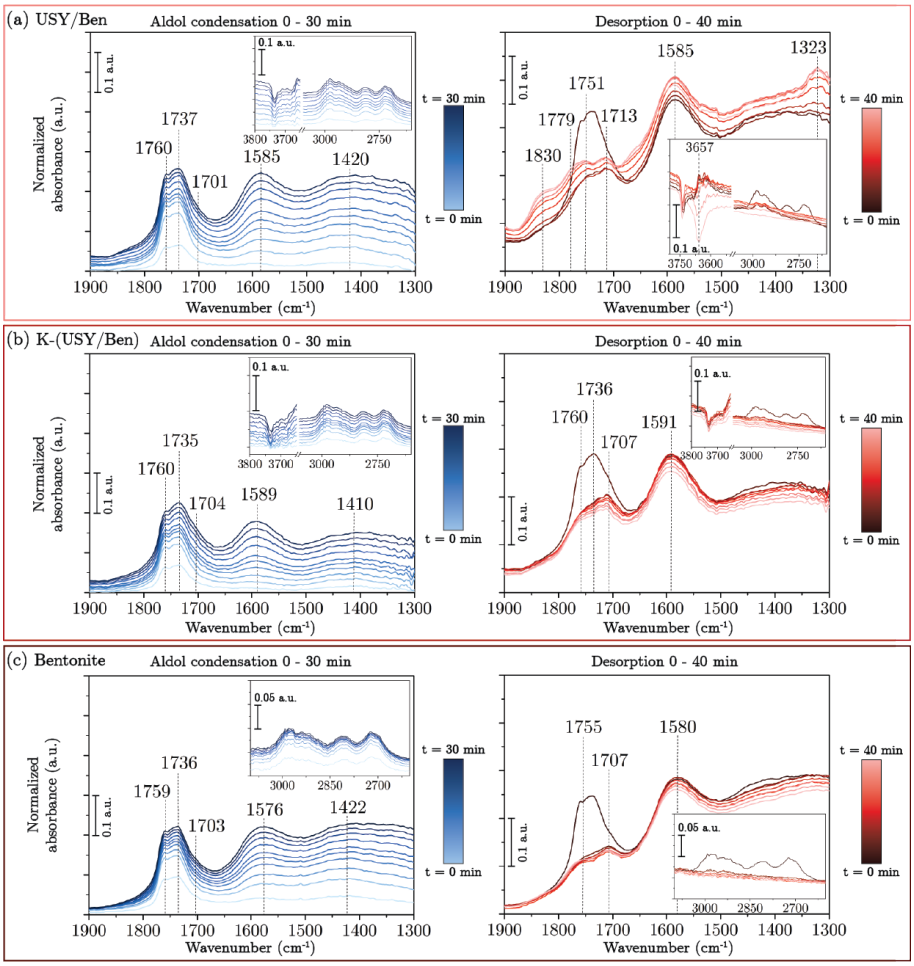

Figure 3.20: Overview of the normalized FT-IR absorbance spectra obtained during reaction and desorption of the aldol condensation of propanal performed at 400 °C using (a) USY/Bentonite, (b) K-(USY/Bentonite) and (c) bentonite as catalyst materials.

To gain more insight in the selectivity of USY/Bentonite, GC-MS analysis was performed on the products collected during reaction. A summary of the obtained results is shown in Table 3.7. It can be seen that both the desired product 2M2P and the main undesired side product 3P are identified. Moreover, six side products not observed in the reference reaction (over K-grafted USY) are identified. The identified species comprise of carboxylic acid and acetate compounds, for example based on acetic acid, pentanoic acid and pentyl acetate. This result points to a high selectivity of USY/Bentonite towards the undesired reaction pathway via the Tishchenko reaction (Scheme 1.3). This cannot be explained by the incorporation of the clay, as in the case of bentonite no peak ascribed to 3P is observed and only three additional side products are identified. Instead the high selectivity towards the undesired pathway could be caused by the weak Brønsted acid site created upon interaction of USY with bentonite.

Upon K-grafting the selectivity of the technical catalyst is improved significantly. This is observed in results obtained by both *in-situ* IR and *ex-situ* GC-MS. In the IR spectra obtained during reaction the formation of aldol condensation products ($\nu_{C=O}$, 1704 cm^{-1}) seems to increase. Additionally, during desorption the formation of additional byproducts seen for USY/Bentonite are no longer observed. With GC-MS analysis the improvement in selectivity is confirmed. The increase in selectivity is mainly observed by a reduction in the amount of additional byproducts from six to only two. Both these side products were oxygenated compounds. Peaks assigned to 2M2P and 3P were identified as well. The intensity of the 2M2P peak does not change upon K-grafting, indicating that the improvement in selectivity is not accompanied by an increase in the yield of aldol condensation products.

Table 3.7: Summary of the results obtained from GC-MS analysis of the reaction mixtures from USY/Bentonite, K-(USY/Bentonite) and bentonite.

Catalyst	2M2P presence	2M2P intensity[a]	3P presence	Additional products[b]
USY/Ben	Yes	2.80	Yes	6
K-(USY/Ben)	Yes	2.56	Yes	2
Bentonite	Yes	2.16	No	3

[a] Compared to the 2M2P peak intensity found for the blanc reaction
[b] Compared to the identified peaks for the K-USY catalyzed reaction

Deactivation The upscaling process influences the deactivation of the technical catalysts as well. It is expected that the incorporation of bentonite results in an increased deactivation. As observed in the IR spectra obtained during desorption of bentonite, the aromatic species ($\nu_{C=C}$, 1580 cm^{-1}) desorb from the surface very slowly. After 40 minutes of desorption as much as 4.0 wt% coke is still present in the spent binder material (Figure 3.19b). Agglomeration and extrusion of USY with bentonite indeed results in an increased deactivation. As seen in the IR spectra obtained during desorption of USY/Bentonite and discussed in the previous section, little desorption of product and aromatic species ($\nu_{C=C}$, 1585 cm^{-1}) is observed, as new species are being formed. Furthermore, the obtained DRS-UV-Vis spectra show that only part of the formed polyaromatics are removed from the USY/Bentonite surface during the desorption (Figure B.7a). This leads to an amount of 2.2 wt% coke present in spent USY/Bentonite extrudates (Figure 3.19b).

In the K-grafted USY/Bentonite catalyst, the resistance against deactivation is slightly improved. As seen in the IR spectra obtained during desorption aromatic species that have formed on the surface during reaction ($\nu_{C=C}$, 1591 cm^{-1}) desorb from the surface slowly but steadily once propanal is desorbed. This results in a low amount of coke present in the spent K-grafted catalyst, only 1.4 wt % in case of an extrudate-shaped catalyst (Figure 3.19b) and 2.1 wt% in case of a wafer-shaped catalyst.

The effect of K-grafting on catalyst deactivation is visualized by CFM. In Figure 3.21 CFM images of a spent USY/Bentonite and K-grafted USY/Bentonite extrudate are shown. It can be observed that less and softer (i.e. H-richer) coke is formed near the edge of the K-grafted catalyst. This correlates with the area in which the presence of Lewis acid sites is reduced due to the incorporation of K^+-cations. Therefore, it is confirmed that K-grafting reduces catalyst deactivation caused by coke formation. This originates from the decrease in the acid sites present in the catalyst. Furthermore, for both extrudates areas showing yellow and green fluorescence are seen, indicating areas that contain soft coke. This effect arises from a reduction in pore accessibility of these domains due to coke formation on the outer surface. Hereby the diffusion of reactants and further coke formation in these areas is prevented, resulting in only a small amount of soft coke. This can be the case with bentonite domains surrounded by USY domains, as it was shown that additional acid sites arise from their interaction, thereby increasing coke formation on the outer surface.

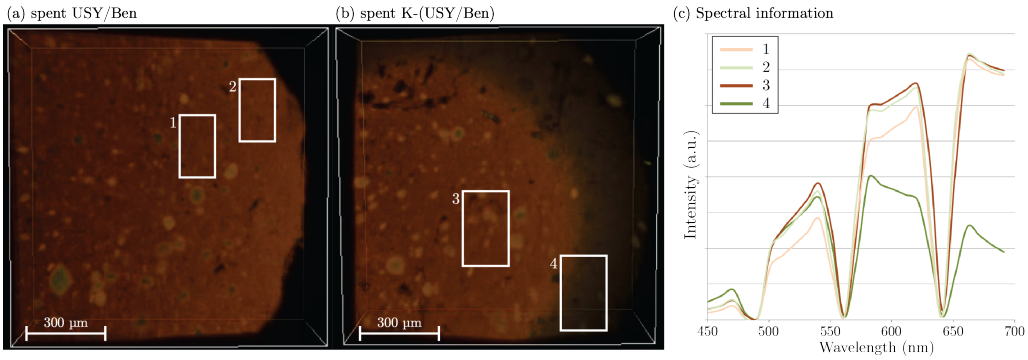

Figure 3.21: Confocal fluorescence microscopy images and spectral information obtained from the cross section of a spent (a) USY/Bentonite and (b) K-(USY/Bentonite) extrudate. λ_{ex} = 404, 488, 561 and 642 nm, detection 450–700 nm.

Shaping effects As previously shown by the differences in coke present in a spent K-grafted bentonite-bound extrudate compared to a spent K-(USY/Bentonite) wafer, the shape of the technical catalyst used in the aldol condensation reaction can influence the catalytic performance of the catalyst. In case of K-grafted USY/Bentonite extrudates the conversion is increased by only 3 % compared to the wafer shaped sample. This increase in conversion is accompanied by a small decrease in catalyst deactivation, as 0.7 wt% less coke is present in the spent extrudate compared to the spent wafer. Overall it seems that the shape of the technical catalyst does not severely impact its performance. The small differences can be explained by a small decrease in catalyst deactivation. This decrease results in a higher activity and higher conversion. Further investigation would be necessary to uncover the cause of the reduced deactivation.

To summarize, in this section it was shown that agglomeration of USY with bentonite increases the propanal conversion and the catalysts selectivity towards the undesired Tishchenko reaction pathway. Additionally, the deactivation of the catalyst due to coke formation is increased. These results are explained by the presence of several active sites in the technical catalyst. Brønsted and Lewis acid sites of intermediate and high strength are introduced by the incorporation of bentonite and additionally, interaction between USY and bentonite results in a new weakly acidic sites. In the technical K-grafted USY/Bentonite catalyst propanal conversion is further increased, selectivity is improved and deactivation due to coke formation is reduced. The latter two observations can be explained by a reduction in acid sites present in the catalyst. The increase in propanal conversion can be explained by the improvement of the catalyst deactivation. As the stability of the catalyst during reaction is improved, it stays more active over time and therefore more propanal is converted.

3.4 Binder effects

In the previous sections the effect of the proposed two-step upscaling procedure on technical catalysts containing attapulgite and bentonite clay has been extensively discussed. It is clear that the choice of binder material can greatly alter the acid and basic properties of the material. Previously, these changes were correlated to the effect they have on the catalytic performance on the catalyst. In the following section the focus will be more on the origin of these changes. For this purpose, a comparison will be made between the effect that each clay has on the acid and basic properties of the technical catalyst in both steps of the upscaling procedure.

3.4.1 Agglomeration and extrusion

In the first step of the upscaling procedure, the agglomeration and extrusion of USY with either attapulgite or bentonite, several active sites are introduced in the technical catalyst in both cases. As these sites originate from incorporation of the binder, the nature and amount of the active sites depends entirely on the nature of the clay.

This effect is illustrated in Figure 3.22 by the IR absorbance spectra in the region between 1650 and 1550 cm^{-1} obtained during pyridine thermodesorption experiments of both binder materials. As explained in more detail in sections 3.2 and 3.3 attapulgite contains several Lewis acid sites, whereas bentonite contains both Brønsted and Lewis acid sites. Additionally, using CO_2-IR it was found that basic sites of intermediate strength were present in different amount in both materials. The origin of the active sites is attributed to the complex nature of the clays. Both consists of over 20 different elements, including Al, Fe, Mg and Na, from which Brønsted and Lewis acid sites as well as basic sites can arise. A more complete overview of the composition of attapulgite and bentonite is given in Appendix B.

Additionally, in the case that USY is mixed and extruded with bentonite as binder material, active sites are not only introduced by the clay, a new active site is also formed due to interaction between USY and bentonite. In literature, the creation of new sites in clay-bound technical catalysts is commonly explained by solid-state cation migration from the clay to extraframework cation positions. However, as in high-silica zeolites only very few of these extraframework positions are present, this does not explain the creation of a new site upon interaction of high-silica USY (Si/Al = 405) with bentonite.

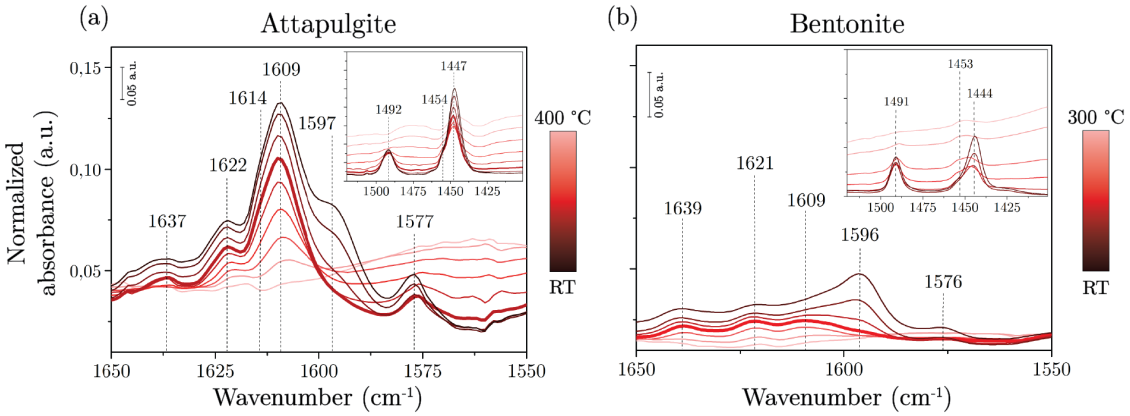

Figure 3.22: Normalized FT-IR spectra of the catalyst materials (a) attapulgite and (b) bentonite during pyridine desorption from room temperature to 400 °C and 300 °C, respectively. The spectra taken at 150 °C are represented in bold.

Moreover, the results discussed in section 3.3 and shown in Figure 3.16 suggest that the new site arises from an increased acidity in surface silanol groups present in USY. This can be explained by the formation of a Si-OH-M bridge between USY and bentonite, where M is a metal present in the clay. In this way, the donor-acceptor interaction between the oxygen atom of the silanol group and the incorporated element M increases, thereby increasing the acidic strength of the silanol group. Several elements present in bentonite can act as element M to form these metallosilicate species, for example Al and Fe.[24]

3.4.2 K-Grafting

The aim of the second step of the upscaling procedure, K-grafting, is the formation of new active sites, in particular basic sites of intermediate strength. In the case of the research catalyst USY it was shown that upon introduction of K^+-cations in the material, basic sites and Lewis acid sites of intermediate strength are created due to the coordination of K^+ to deprotonated silanol groups (Section 3.1). Interestingly, the effect that K-grafting has on technical USY/Clay catalysts depends on the nature of the binder.

In case of the technical USY/Attapulgite catalyst, the introduction of K^+ results in the formation of active sites that are similar to those created in the research catalyst. This is in contrast with bentonite-bound technical catalyst. Here the introduction of K^+ results in a reduction of active sites. This difference can be explained by the different nature of the used binder materials. In Figure 3.23 the IR absorbance in the OH-stretching region of both attapulgite and bentonite is shown. The grafting procedure consists of the deprotonation of surface silanol sites followed by the coordination of K^+-ions to the deprotonated site. It is therefore interesting to compare the surface-OH groups that are present in attapulgite and bentonite. As clearly observed, bentonite contains many surface-OH groups, whereas attapulgite contains significantly less.

This can explain the difference in behavior upon K-grafting. In the case of the attapulgite-bound technical catalyst the majority of the incorporated K^+ will interact with the silanol groups present in USY. Thereby basic and Lewis acid sites of intermediate strength similar to those present in K-grafted USY are created. On the other hand, upon introduction of K^+ in the bentonite-bound technical catalyst a major part of the incorporated K^+-cations will interact with surface-OH groups present in the binder. In this way, H^+ and other cations that form the Brønsted and Lewis acid sites present in the binder are replaced and the amount of acid sites in the technical USY/Bentonite catalyst is reduced.

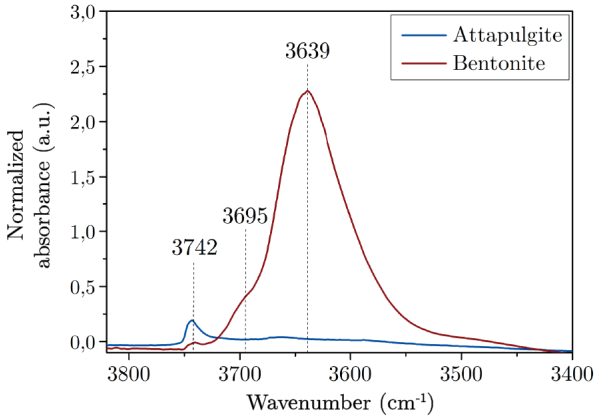

Figure 3.23: Normalized IR absorbance spectrum of attapulgite and bentonite dried under vacuum in the region between 3820 and 3600 cm^{-1}.

Overall, the use of attapulgite as binder material offers higher control over the creation of active sites in the final K-grafted technical catalyst than bentonite clay. As control over the active sites present in the catalyst, allows for good control over its catalytic performance, K-grafted USY/Attapulgite seems the most promising technical catalyst for the upgrading of bio-oil via the aldol condensation reaction.

Chapter 4

Conclusion and Outlook

By using *operando* and *in-situ* measurements combined with on-line MS and off-line GC, respectively, in combination with several *ex-situ* characterization methods the effect of upscaling on technical clay-bound USY catalysts has been studied. The results indicate that with the proposed two-step upscaling procedure, consisting of extrusion of USY with a clay binder and K-grafting, it is possible to obtain stable K-grafted USY/Attapulgite and USY/Bentonite technical catalysts. For both catalysts, the two upscaling steps have a significant impact on the catalytic performance, i.e. the activity, selectivity and stability of the catalyst.

In the first step of the upscaling procedure, the agglomeration and extrusion of USY with either attapulgite or bentonite, extrudate-shaped USY/clay catalyst particles are obtained. For both binder materials, the crystallographic structure and pore structure remain largely intact as demonstrated by XRD and Ar physisorption. Additionally, using CO_2-IR and Py-IR analyses combined with fluorescein stained extrudates studied by CFM, it was found that active sites present in the clay are incorporated in the clay-bound technical catalysts. Moreover, in the case of bentonite-bound catalyst, the interaction of USY with bentonite results in the formation of a new active site of weak acidic strength. Overall, due to the presence of several active sites in the extrudates obtained in the first step of the upscaling procedure the technical catalysts are more active. However, the non-grafted technical catalysts are less selective towards the aldol condensation pathway and less stable against catalyst deactivation due to coke formation. This was observed during *operando* measurements combined with on-line MS and *in-situ* measurements combined with off-line GC. Furthermore, these results were confirmed with TGA and CFM analysis of the spent extrudate samples.

The second step of the upscaling procedure, K-grafting, has a different influence on the catalyst depending on the binder material used. In the case of the attapulgite-bound technical catalyst, basic and Lewis acid sites of intermediate strength are created upon K-grafting. Using CO_2- and Py-IR studies, it was possible to confirm that the created sites are similar to those present in the K-grafted USY research catalyst. Furthermore, *in-situ* IR data combined with *ex-situ* GC-MS analyses of the reaction products showed that the formation of these sites increases the selectivity of the catalyst towards the desired aldol condensation pathway. On the other hand, in the case of the bentonite-bound technical catalyst, no new sites seem to be created upon K-grafting. Instead, it was observed with Py-IR that active sites present in the non-grafted USY/Bentonite catalyst are removed from the catalyst during the grafting procedure. With GC-MS analysis of catalyst selectivity in combination with TGA and CFM analyses of the spent sample, it was observed that the removal of these sites decreases the selectivity towards the undesired Tishchenko pathway and reduces catalyst deactivation due to coke formation.

To conclude, both steps of the upscaling procedure significantly affect the properties and performance of the catalyst. This impact mainly originates from the nature of the chosen binder material. The influence of the binder material might be minimized by the incorporation of a binder with little intrinsic active sites and that allows for control over the creation of additional active sites, for example by K-grafting. In this way, it could be possible to optimize control over the catalytic performance of the technical catalyst.

Outlook

In this section, several recommendations to improve and to complement this study are given. First of all, the catalytic results discussed in this thesis could be improved by the collection of more accurate quantitative GC data on the activity and selectivity of the catalysts. The acquisition of data with off-line GC was difficult and suffered from unavoidable experimental errors. This could be improved significantly if the GC data would have been collected on-line during *operando* measurements.

Secondly, with IR microscopy spatiotemporal *operando* measurements could be performed on extrudate-shaped catalysts instead of representative wafer-shaped catalysts. The reaction cell available during this study was not suitable for studying extrudates and therefore the performed *in-situ* IR microscopy experiments did not yield spectra with sufficiently good resolution. Improvement of this data, for example by implementation of a suitable cell, would provide valuable insight in the selectivity and stability of the shaped catalysts. Moreover, *in-situ* IR microscopy mapping might enable the correlation of the product formation of the technical catalyst with the distribution of active sites observed by CFM.

A complementary study on K-grafting would provide insightful information on the grafting process and zeolite-binder interactions. This could be studied by addition of several new catalytic materials to the studied series. To gain more insight on the effect of K-grafting on the previously studied technical catalysts, non-grafted USY/Attapulgite, K-grafted attapulgite and K-grafted bentonite could be studied. Furthermore, to study the influence that the nature of the binder material has on the effect of K-grafting the addition of a third clay to the series, for example kaolin, would be interesting. Finally, the effect of the weight percentage K incorporated in the K-grafted catalysts could be studied by improving control over the K-grafting procedure.

Acknowledgements

During this project there were a lot of people who helped me with my research, who I would like to thank. First of all, I would like to thank my daily supervisor Ana Hernández Giménez. I enjoyed working together a lot. You were always ready to discuss new results and to help when necessary, but you also let me make this project my own. Thank you for that! Gracias y suerte en los próximos meses!

Secondly, I would like to thank Pieter Bruijnincx and Gareth Whiting. Pieter, thank you for your supervision, feedback on my work and presentations and your help, not only with the project, but also with my internship. Gareth, thank you for your supervision and help, in particular with the synthesis of the bentonite-bound extrudates.

Furthermore, I would like to thank the people who helped me with several characterization techniques used during my project. Marjan Versluijs-Helder helped me with the execution of the TGA measurements. Jochem Wijten helped me a lot by performing SEM-EDX measurements. Miguel Rivera Torrente and Sander Lambregts provided me with the Ar physisorption data. Helen de Waard helped me with the execution of ICP-OES measurements.

Finally, I would like to thank the other master students, in particular Frederique Broers, Thomas van Swieten, Lucas Teunissen, David Verbart and Nienke Visser, for all the good times, support and coffee and snack breaks. You made the long days go by a lot faster! And last but not least, I would like to thank Joost, for supporting me and having the patience to listen when I wanted to show off my results and practice presentations!

Bibliography

[1] European Commission, "Renewable energy." `http://ec.europa.eu/energy/en/topics/renewable-energy`, 2017. Last accessed: 2017-11-25.

[2] I. Graça, J. M. Lopes, H. S. Cerqueira, and M. F. Ribeiro, "Bio-oils Upgrading for Second Generation Biofuels," *Industrial & Engineering Chemistry Research*, vol. 52, no. 1, pp. 275—-287, 2013.

[3] M. F. Demirbas, M. Balat, and H. Balat, "Potential contribution of biomass to the sustainable energy development," *Energy Conversion and Management*, vol. 50, no. 7, pp. 1746–1760, 2009.

[4] P. M. Mortensen, J. Grunwaldt, P. A. Jensen, K. G. Knudsen, and A. D. Jensen, "A review of catalytic upgrading of bio-oil to engine fuels," *Applied Catalysis A, General*, vol. 407, no. 1-2, pp. 1–19, 2011.

[5] Q. Zhang, J. Chang, T. Wang, and Y. Xu, "Review of biomass pyrolysis oil properties and upgrading research," *Energy conversion and management*, vol. 48, no. 1, pp. 87–92, 2007.

[6] B. Puértolas, T. C. Keller, S. Mitchell, and J. Pérez-Ramírez, "Deoxygenation of bio-oil over solid base catalysts: From model to realistic feeds," *Applied Catalysis B: Environmental*, vol. 184, pp. 77–86, 2016.

[7] T. P. Vispute, H. Zhang, A. Sanna, R. Xiao, and G. W. Huber, "Renewable chemical commodity feedstocks from integrated catalytic processing of pyrolysis oils," *Science*, vol. 330, no. 6008, pp. 1222–1227, 2010.

[8] T. C. Keller, E. G. Rodrigues, and J. Pérez-Ramírez, "Generation of Basic Centers in High-Silica Zeolites and their Application in Gas-Phase Upgrading of Bio-Oil," *ChemSusChem*, vol. 7, no. 6, pp. 1729–1738, 2014.

[9] R. W. Snell, E. Combs, and B. H. Shanks, "Aldol condensations using bio-oil model compounds: the role of acid–base bi-functionality," *Topics in Catalysis*, vol. 53, no. 15-18, pp. 1248–1253, 2010.

[10] X. Zhu, L. L. Lobban, R. G. Mallinson, and D. E. Resasco, "Tailoring the mesopore structure of HZSM-5 to control product distribution in the conversion of propanal," *Journal of Catalysis*, vol. 271, no. 1, pp. 88–98, 2010.

[11] M. Milina, S. Mitchell, and J. Pérez-Ramírez, "Prospectives for bio-oil upgrading via esterification over zeolite catalysts," *Catalysis Today*, vol. 235, pp. 176–183, 2014.

[12] J. E. McMurry, *Organic Chemistry.* Cengage Learning, 8th ed., 2012. pp. 905-915.

[13] J. Clayden, N. Greeves, and S. Warren, *Organic Chemistry.* Oxford University Press. UK, 2nd ed., 2012.

[14] D. Mohan, C. U. Pittman, and P. H. Steele, "Pyrolysis of wood/biomass for bio-oil: a critical review," *Energy & fuels*, vol. 20, no. 3, pp. 848–889, 2006.

[15] Z. He and X. Wang, "Hydrodeoxygenation of model compounds and catalytic systems for pyrolysis bio-oils upgrading," *Catalysis for sustainable energy*, vol. 1, pp. 28–52, 2013.

[16] J. I. Di Cosimo and C. R. Apesteguía, "Study of the catalyst deactivation in the base-catalyzed oligomerization of acetone," *Journal of Molecular Catalysis A: Chemical*, vol. 130, no. 1, pp. 177–185, 1998.

[17] H. Hattori, "Heterogeneous basic catalysis," *Chemical Reviews*, vol. 95, no. 3, pp. 537–558, 1995.

[18] M. Asadieraghi, W. M. A. W. Daud, and H. F. Abbas, "Model compound approach to design process and select catalysts for in-situ bio-oil upgrading," *Renewable and Sustainable Energy Reviews*, vol. 36, pp. 286–303, 2014.

[19] T. C. Keller, K. Desai, S. Mitchell, and J. Pérez-Ramírez, "Design of base zeolite catalysts by alkali-metal grafting in alcoholic media," *Acs Catalysis*, vol. 5, no. 9, pp. 5388–5396, 2015.

[20] J. Weitkamp, "Zeolites and catalysis," *Solid State Ionics*, vol. 131, no. 1, pp. 175–188, 2000.

[21] Y. Wei, T. E. Parmentier, K. P. de Jong, and J. Zecevic, "Tailoring and visualizing the pore architecture of hierarchical zeolites," *Chemical Society Reviews*, vol. 44, no. 20, pp. 7234–7261, 2015.

[22] B. Smit and T. L. Maesen, "Towards a molecular understanding of shape selectivity," *Nature*, vol. 451, no. 7179, p. 671, 2008.

[23] J. N. Kondo, R. Nishitani, E. Yoda, T. Yokoi, T. Tatsumi, and K. Domen, "A comparative ir characterization of acidic sites on HY zeolite by pyridine and CO probes with silica–alumina and γ-alumina references," *Physical Chemistry Chemical Physics*, vol. 12, no. 37, pp. 11576–11586, 2010.

[24] E. Derouane, J. C. Vedrine, R. R. Pinto, P. Borges, L. Costa, M. Lemos, F. Lemos, and F. R. Ribeiro, "The acidity of zeolites: concepts, measurements and relation to catalysis: a review on experimental and theoretical methods for the study of zeolite acidity," *Catalysis Reviews*, vol. 55, no. 4, pp. 454–515, 2013.

[25] S. Bordiga, C. Lamberti, F. Bonino, A. Travert, and F. Thibault-Starzyk, "Probing zeolites by vibrational spectroscopies," *Chemical Society Reviews*, vol. 44, no. 20, pp. 7262–7341, 2015.

[26] A. Corma, V. Fornes, R. Martin-Aranda, H. Garcia, and J. Primo, "Zeolites as base catalysts: condensation of aldehydes with derivatives of malonic esters," *Applied catalysis*, vol. 59, no. 1, pp. 237–248, 1990.

[27] D. Barthomeuf, "Framework induced basicity in zeolites," *Microporous and mesoporous materials*, vol. 66, no. 1, pp. 1–14, 2003.

[28] T. C. Keller, M. Položij, B. Puértolas, H. V. Thang, P. Nachtigall, and J. Perez-Ramirez, "Understanding the structure of cationic sites in alkali metal-grafted USY zeolites," *The Journal of Physical Chemistry C*, vol. 120, no. 9, pp. 4954–4960, 2016.

[29] Cascatbel Project, "About cascatbel." `http://www.cascatbel.eu/project/`, 2013. Last accessed: 2017-10-19.

[30] S. Mitchell, N.-L. Michels, and J. Pérez-Ramírez, "From powder to technical body: the undervalued science of catalyst scale up," *Chemical Society Reviews*, vol. 42, no. 14, pp. 6094–6112, 2013.

[31] G. T. Whiting, F. Meirer, M. M. Mertens, A.-J. Bons, B. M. Weiss, P. A. Stevens, E. de Smit, and B. M. Weckhuysen, "Binder effects in SiO_2- and Al_2O_3-bound zeolite ZSM-5-based extrudates as studied by microspectroscopy," *ChemCatChem*, vol. 7, no. 8, pp. 1312–1321, 2015.

[32] B. Kraushaar-Czarnetzki and S. P. Muller, "Shaping of solid catalysts," *Synthesis of Solid Catalysts*, 2009.

[33] M. Campanati, G. Fornasari, and A. Vaccari, "Fundamentals in the preparation of heterogeneous catalysts," *Catalysis Today*, vol. 77, no. 4, pp. 299–314, 2003.

[34] G. T. Whiting, A. D. Chowdhury, R. Oord, P. Paalanen, and B. M. Weckhuysen, "The curious case of zeolite–clay/binder interactions and their consequences for catalyst preparation," *Faraday discussions*, vol. 188, pp. 369–386, 2016.

[35] J. Hargreaves and A. Munnoch, "A survey of the influence of binders in zeolite catalysis," *Catalysis Science & Technology*, vol. 3, no. 5, pp. 1165–1171, 2013.

[36] R. V. Jasra, B. Tyagi, Y. M. Badheka, V. N. Choudary, and T. S. Bhat, "Effect of clay binder on sorption and catalytic properties of zeolite pellets," *Industrial & engineering chemistry research*, vol. 42, no. 14, pp. 3263–3272, 2003.

[37] A. de Lucas, J. L. Valverde, P. Sánchez, F. Dorado, and M. J. Ramos, "Influence of the binder on the n-octane hydroisomerization over palladium-containing zeolite catalysts," *Industrial & engineering chemistry research*, vol. 43, no. 26, pp. 8217–8225, 2004.

[38] P. Sánchez, F. Dorado, A. Fúnez, V. Jiménez, M. J. Ramos, and J. L. Valverde, "Effect of the binder content on the catalytic performance of beta-based catalysts," *Journal of Molecular Catalysis A: Chemical*, vol. 273, no. 1, pp. 109–113, 2007.

[39] F. Dorado, R. Romero, and P. Cañizares, "Hydroisomerization of n-butane over Pd/HZSM-5 and Pd/Hβ with and without binder," *Applied Catalysis A: General*, vol. 236, no. 1, pp. 235–243, 2002.

[40] N.-L. Michels, S. Mitchell, and J. Pérez-Ramìrez, "Effects of binders on the performance of shaped hierarchical MFI zeolites in methanol-to-hydrocarbons," *ACS Catalysis*, vol. 4, no. 8, pp. 2409–2417, 2014.

[41] J. Lavalley, "Infrared spectrometric studies of the surface basicity of metal oxides and zeolites using adsorbed probe molecules," *Catalysis Today*, vol. 27, no. 3-4, pp. 377–401, 1996.

[42] J. Datka, A. Turek, J. Jehng, and I. Wachs, "Acidic properties of supported niobium oxide catalysts: an infrared spectroscopy investigation," *Journal of Catalysis*, vol. 135, no. 1, pp. 186–199, 1992.

[43] H. Knözinger, "Infrared spectroscopy for the characterization of surface acidity and basicity," *Handbook of Heterogeneous Catalysis*, 1997.

[44] H. Zhang, S. Shao, R. Xiao, D. Shen, and J. Zeng, "Characterization of coke deposition in the catalytic fast pyrolysis of biomass derivates," *Energy & Fuels*, vol. 28, no. 1, pp. 52–57, 2013.

[45] C. Emeis, "Determination of integrated molar extinction coefficients for infrared absorption bands of pyridine adsorbed on solid acid catalysts," *Journal of Catalysis*, vol. 141, no. 2, pp. 347–354, 1993.

[46] G. Socrates, *Infrared and Raman characteristic group frequencies: tables and charts*. John Wiley & Sons, 2004.

[47] P. Kalsi, *Spectroscopy of organic compounds*. New Age International, 2007. pp. 1-160.

[48] J. W. Niemantsverdriet, *Spectroscopy in catalysis*. John Wiley & Sons, 3rd ed., 2007. pp. 217–247.

[49] H. Knözinger and S. Huber, "Ir spectroscopy of small and weakly interacting molecular probes for acidic and basic zeolites," *Journal of the chemical society, faraday transactions*, vol. 94, no. 15, pp. 2047–2059, 1998.

[50] A. M. Hernández-Giménez, J. Ruiz-Martínez, B. Puértolas, J. Pérez-Ramírez, P. C. Bruijnincx, and B. M. Weckhuysen, "Operando spectroscopy of the gas-phase aldol condensation of propanal over solid base catalysts," *Topics in Catalysis*, pp. 1–15, 2017.

[51] D. C. Harris, *Quantitative Chemical Analysis*. W.H.Freeman & Co Ltd, 7th ed., 2007. pp. 506-555.

[52] E. Stavitski, M. H. Kox, and B. M. Weckhuysen, "Revealing shape selectivity and catalytic activity trends within the pores of H-ZSM-5 crystals by time-and space-resolved optical and fluorescence microspectroscopy," *Chemistry-A European Journal*, vol. 13, no. 25, pp. 7057–7065, 2007.

[53] D. Semwogerere and E. R. Weeks, "Confocal microscopy," *Encyclopedia of Biomaterials and Biomedical Engineering*, vol. 23, pp. 1–10, 2005.

[54] A. N. Parvulescu, D. Mores, E. Stavitski, C. M. Teodorescu, P. C. Bruijnincx, R. J. K. Gebbink, and B. M. Weckhuysen, "Chemical imaging of catalyst deactivation during the conversion of renewables at the single particle level: etherification of biomass-based polyols with alkenes over H-beta zeolites," *Journal of the American Chemical Society*, vol. 132, no. 30, pp. 10429–10439, 2010.

[55] D. Mores, J. Kornatowski, U. Olsbye, and B. M. Weckhuysen, "Coke formation during the methanol-to-olefin conversion: In situ microspectroscopy on individual H-ZSM-5 crystals with different brønsted acidity," *Chemistry-A European Journal*, vol. 17, no. 10, pp. 2874–2884, 2011.

[56] G. T. Whiting, F. Meirer, D. Valencia, M. M. Mertens, A.-J. Bons, B. M. Weiss, P. A. Stevens, E. De Smit, and B. M. Weckhuysen, "Selective staining of brønsted acidity in zeolite ZSM-5-based catalyst extrudates using thiophene as a probe," *Physical Chemistry Chemical Physics*, vol. 16, no. 39, pp. 21531–21542, 2014.

[57] L. R. Aramburo, J. Ruiz-Martínez, J. P. Hofmann, and B. M. Weckhuysen, "Imaging the effect of a hydrothermal treatment on the pore accessibility and acidity of large ZSM-5 zeolite crystals by selective staining," *Catalysis Science & Technology*, vol. 3, no. 5, pp. 1208–1214, 2013.

Appendix A

Experimental techniques

The properties and catalytic performance of the catalysts were studied using several techniques, including Infrared Spectroscopy (FT-IR), Gas Chromatography (GC), Mass Spectrometry (MS) and Confocal Fluorescence Microscopy (CFM). In this chapter the theoretical background of these techniques will be briefly discussed.

A.1 Fourier Transfer-Infrared Spectroscopy

In this thesis Fourier Transfer-Infrared (FT-IR) spectroscopy has been used to study the aldol condensation reaction over the catalyst *in-situ* and to determine the nature of the acid and basic sites with CO_2- and pyridine-IR. In this section the basic concepts of IR spectroscopy will be covered, after which more details on CO_2- and pyridine-IR spectroscopy and *in-situ* IR analysis will be given.

Spectroscopy techniques are based on the interaction of matter with electromagnetic radiation. More specifically, the absorption of electromagnetic radiation of a specific energy that matches the transition energy of an electron from a low energy state to a higher energy state within that matter. Each region of the electromagnetic spectrum interacts differently with molecules. For example, when radiation in the UV-Vis region interacts with a molecule, the absorption of light results in the promotion of an electron from the HOMO to the LUMO. Whereas if radiation in the IR region is absorbed by a molecule, this changes the vibrational and rotational movements of the molecule. The energy necessary for these transition depends on the properties of that molecule, for example the bond strength or mass of the atoms.[47,48]

As the name already states, IR spectroscopy is a technique in which the interaction of the infrared region of the electromagnetic spectrum with the system of interest is studied. The infrared region of the electromagnetic spectrum ranges from wavelengths of 1 mm in the near-IR to 750 nm in the far-IR. There are several different IR spectroscopy techniques, e.g. diffuse reflection, emission, scattering and transmission. The latter technique is used in this thesis. For this technique, IR radiation is allowed to pass through the sample, after which the transmitted infrared radiation is detected. From the spectrum of the transmitted radiation, it can be seen at which wavelength radiation is adsorbed by the sample. Because only radiation corresponding to specific energy transitions in the sample is absorbed, a molecular fingerprint of the material can be made. This provides information about the composition and structure of the material, i.e. what bonds are present in the material.[47,48] Using this information, it is possible to determine the structural composition of the sample or changes on the surface of the material during in−situ experiments.

A.1.1 CO_2-IR

CO_2-IR is a commonly used technique to determine the nature of basic sites present in a material. It builds on the fact that the mildly acid CO_2 molecule can interact with the basic sites present in the material. The complexes formed on the surface give rise to specific IR absorbance bands, that can be used to gain insight on the studied material.

In zeolites, CO_2 can interact with different components in the system, namely on basic hydroxyl groups, basic oxygen ions and extraframework cations.[41,49] Most interesting for this work is the interaction of CO_2 with basic oxygen centers. This interaction results in the formation of carbonate

species, as is illustrated in Figure A.1. A free carbonate has an asymmetric stretching vibration ν_3 at 1415 cm^{-1}. When a carbonate is absorbed on a surface, the ν_3 vibration splits in two vibrations with $\Delta\nu_3$ that can be observed in the range of 1300 - 1700 cm^{-1}.[25,41] Depending on the strength of the interaction between CO_2 and the basic site, different carbonate species form that can be differentiated by the value of $\Delta\nu_3$. Unidentate carbonates ($\Delta\nu_3$ < 150 cm^{-1}) are typically formed on strong basic sites, whereas bidentate carbonates ($\Delta\nu_3$ = 150 - 400 cm^{-1}) form on sites of intermediate basic strength.[41]

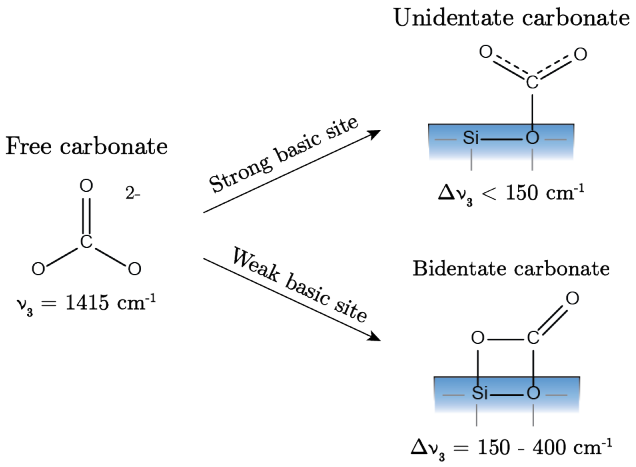

Figure A.1: Schematic representation of a free carbonate and the carbonate complexes forming upon interaction of CO_2 with strong and weak to intermediate basic sites. Based on ref.[41]

In addition to the interaction with basic oxygen ions, CO_2 can form linear complexes with extraframework cations, which leads to intense bands around 2360 cm^{-1} due to the asymmetric stretching mode ν_3 of CO_2. Typically this band shifts to lower wavenumber with increasing size and polarizability of the cation. Furthermore, a weak band can be observed near 1370 cm^{-1}, which is attributed to the activated symmetric stretching mode ν_1.[25,49]

A.1.2 Pyridine-IR

Following the adsorption of pyridine on a surface is a useful technique to determine the nature and amount of both Brønsted and Lewis acid sites present in a material. It builds on the fact that the mildly basic pyridine molecule can interact with the acid sites present in the material. The complexes formed on the surface give rise to specific IR absorbance bands, that provide insight on the properties of the studied material.

Upon interaction of pyridine with different surface acid sites, different pyridine complexes are formed, which are illustrated in Figure A.2. The original vibrational modes of pyridine, ν_{19b} and ν_{8a} at 1439 and 1583 cm^{-1}, are mostly affected by these interactions. In Table A.1 the vibrational modes for the different pyridine complexes absorbed on a surface are shown.

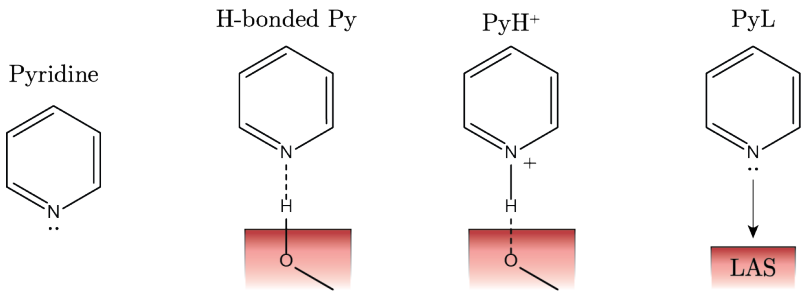

Figure A.2: Schematic representation of free pyridine and the pyridine complexes forming upon interaction with Brønsted and Lewis acid sites. Based on ref.[43]

Table A.1: Characteristic vibrational modes of pyridine and pyridine complexes. Adapted from ref.[43]

Vibration	Pyridine	H-bonded Py	PyH^+	PyL
ν_{19a} (cm^{-1})	1439	1487	1488	1493
ν_{19b} (cm^{-1})	1478	1440 - 1450	1540 - 1550	1440 - 1460
ν_{8a} (cm^{-1})	1583	1580 - 1600	1640	1600 -1635
ν_{8b} (cm^{-1})	1572	1577	1610	1577

Most importantly, the pyridinium ion (PyH^+) obtained from the reaction of pyridine with relatively strong Brønsted acid sites shows bands around 1540-1550 (ν_{19b}) and 1640 (ν_{8a}), whereas pyridine interacting with weak Brønsted acid sites (H-bonded Py) is characterized by bands around 1440-1450 (ν_{19b}) and 1580-1600 cm^{-1} (ν_{8a}). Furthermore, coordinatively bound pyridine on Lewis acid sites (PyL) shows bands around 1440-1460 cm^{-1} (ν_{19b}) and 1600-1635 cm^{-1} (ν_{8a}). Information on the nature and strength of Brønsted and Lewis acid sites can be obtained from pyridine thermodesorption experiments, as this allows distinguition between the different complexes.[42,43] Additionally, the amount of Brønsted and Lewis acid sites can be derived from the characteristic bands around 1545 and 1455 cm^{-1}, respectively. The concentration of acid sites in the material is obtained by using the following equations:

$$C(B) = 1.88 IA(B) R^2 / W$$

$$C(L) = 1.42 IA(L) R^2 / W$$

Here, $C(B, L)$ corresponds to the concentration of either Brønsted (B) or Lewis (L) acid sites in mmol g^{-1} material, $IA(B, L)$ is the integrated absorbance of the IR band corresponding to pyridine adsorbed on Brønsted or Lewis acid sites and R and W are the radius and weight of the catalyst disk, respectively.[45]

A.1.3 *In-situ* IR analysis

Using *in-situ* IR spectroscopy the adsorption of propanal and the formation of products was followed during reaction and desorption. For the interpretation of the IR bands Table A.2 was used.

Table A.2: Characteristic IR bands of propanal and products obtained in the gas-phase condensation of propanal reacting at 400 °C. Adapted from ref. [50].

Position (cm^{-1})	Assignment	Species
3050 - 3080	ν_{C-H}	Aromatics/olefins
2923 - 2986	ν_{C-H}	Propanal/aldol dimer
2940	ν_{C-H}	Propanal/aldol dimer
2905 - 2926[a]	ν_{C-H}	Propanal
2810 - 2855; 2718 - 2726	ν_{C-H} (doublet)	Propanal/aldol dimer
1759 -1763; 1735	$\nu_{C=O}$ (doublet)	Propanal
1709 - 1717	$\nu_{C=O}$	3-Pentanone
1687 - 1706	$\nu_{C=O}$	Aldol dimer/trimer
1670 - 1690	$\nu_{C=C}$	Aldol dimer
1573 - 1590	$\nu_{C=C}$	Aromatics/coke
1395; 1410	σ_{C-H}	Propanal/aldol dimer
1362; 1381	σ_{C-H}	Propanal/aldol dimer

[a] Multiple bands

A.2 Gas Chromatography

In general, chromatography techniques are based on the separation of the components of a mixture by selective adsorption in with a stationary phase. An example is illustrated in Figure A.3. Here, a solution of two compounds A and B is placed on top of a column. Once the outlet of the column is opened A and B will flow down in the column. The mixture is washed down the column by a continuous solvent flow applied on the top of the column, the mobile phase. If compound A more strongly adsorbs on the stationary phase in the column than compound B, then solute A will move through the column more slowly. In this way compound A and B are separated and will emerges from the column after different retention times.[51]

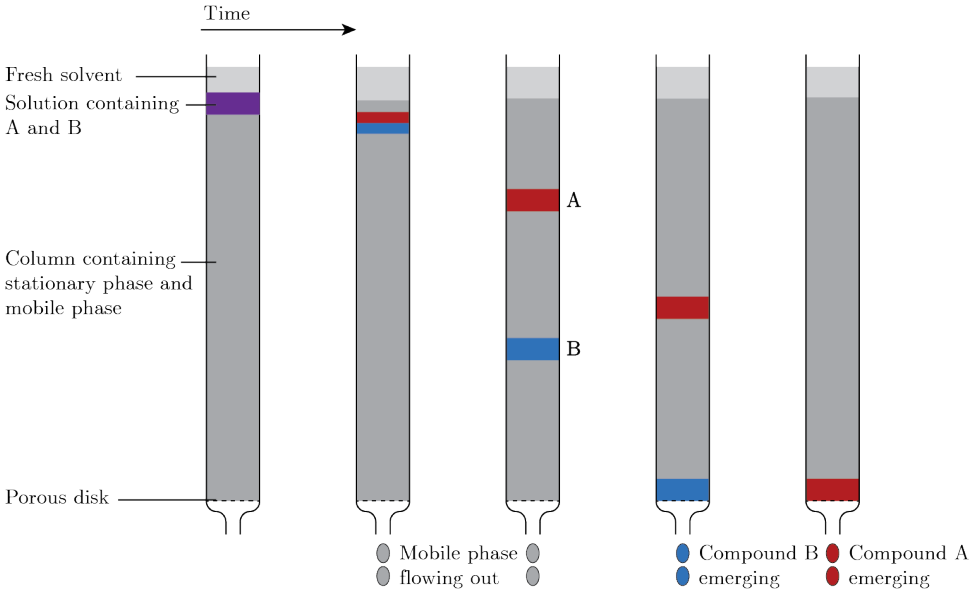

Figure A.3: Schematic representation of the principle behind chromatography. Compound A remains in the column longer then compound B as it has a greater affinity with the stationary phase in the column. Adapted from ref.[51].

Gas Chromatography (GC) is a chromatography technique in which a volatile liquid or gaseous solute is carried over a stationary phase on the inside of a column or on a solid support within the column by a gaseous mobile phase, called the carrier gas. The analyzed sample is injected through a septum into a heated port, in which it rapidly evaporates to form a gas vapor. The vapor is carried further into the column by the carrier gas. Here, the different compounds in the vapor are separated according to their affinity with the column's stationary phase. The separated solutes flow through the detector where they recorded and visualized in a chromatograph.

A.3 Mass Spectrometry

Mass spectrometry (MS) is a technique that is commonly used to study the masses of atoms and molecules, either from pure compounds or present in a mixture. Generally, in a mass spectrometer chemical species are ionized and sorted based on their mass to charge ratio. The abundance of each ion type is detected, thereby creating a specific mass spectrum for the analyzed sample.[51]

In the first step of a mass spectrometry analysis the studied compound (M) is ionized by bombardment with electrons. The interactions of the fast moving electron with a molecule causes the molecule to lose an electron and become positively charged.

$$M + e^- \rightarrow M^{+\cdot} + 2e^-$$

Upon ionization the newly formed molecular cation ($M^{+\cdot}$) can break down to form smaller fragments that are either neutral or positively charged. Following, the obtained ions are transported to a mass analyzer by application of an electric or magnetic field. Due to their different mass-to-charge ratio ($\frac{m}{z}$) the ions respond differently to this field, making it possible to separate them by this ratio.[51]

This can be understood using Lorentz force law and Newton's second law.

$$\mathbf{F} = Q(\mathbf{E} + \mathbf{v} \times \mathbf{B})$$

$$\mathbf{F} = m\mathbf{a}$$

$$\frac{m}{Q}\mathbf{a} = (\mathbf{E} + \mathbf{v} \times \mathbf{B})$$

The resulting relation shows how a charged particle is affected by an electronic or magnetic field, depending on the mass and the charge of that particle. In general, $\frac{m}{Q}$ is rewritten to $\frac{m}{z}$ using $z = \frac{Q}{e}$. In a mass spectrometer different mass analyzers can be used to exploit the relation between $\frac{m}{z}$ and the external field.[51]

Finally, after the ions are sorted by their mass-to-charge ratio, they reach the detector where they are recorded and quantified. In this way a mass spectrum is obtained from the analyzed sample. Different information can be derived from such a mass spectrum. When a pure substance is analyzed it is possible to get a qualitative idea about the structure of the analyzed molecule. Moreover, when a mixture is analyzed using MS the different compounds present in the mixture can be derived. As it can be difficult to analyze complex mixtures, MS analysis is often combined with GC analysis in a GC-MS. In this case, the gas chromatograph separates the components in the mixture, while the mass spectrometer identifies the peaks by creating individual mass spectra. The combination of GC with MS analysis is particularly interesting, as this makes it possible to quantify the compounds present in reaction mixtures in addition to qualitative analysis.

In this study, *on-line* MS was used to follow the formation of products during reaction and desorption over time. Table A.3 gives an overview of the different $\frac{m}{z}$ fragments that are obtained from propanal and the products that form during the gas-phase condensation of propanal at 400 °C. The $\frac{m}{z}$ values that were used to study product selectivity and product formation over time are shown in bold.

Table A.3: Overview of $\frac{m}{z}$ fragments obtained from propanal and the main products obtained in the gas-phase condensation of propanal reacting at 400 °C. Adapted from ref. [50].

Compound	$\frac{m}{z}$ fragments
Propanal	**58**, 57, 29, 28, 27
Aldol dimer (2M2P)	98, 69, **41**
Aldol dimer i.m.[a]	**116**, 87, 59, 57, 29
Aldol trimer	138, **109**, 69, 41
3-Pentanone	**86**, 57, 29
Propyl propionate	87, **75**, 57, 29, 27
Water	**18**, 17

[a] Aldol dimer intermediate (3-hydroxy-2-methylpentanal)

A.4 Confocal Fluorescence Microscopy

Confocal fluorescence microscopy (CFM) is a microscopy technique that is based on a fundamentally different technique compared to conventional microscope techniques. This gives the confocal fluorescence microscope several advantages, such as a high resolution and the ability to obtain 3D reconstructions.[52] In Figure A.4 the general working principle of a confocal fluorescence microscope is schematically illustrated. Firstly, laser light is focused onto the sample. The fluorescence light emitted from the sample, as well as the scattered laser light is then collected by the microscope's objective lens. The scattered excitation light is reflected off using a dichroic mirror, while the fluorescent light goes through the dichroic mirror to the detector. The high resolution in CFM is achieved using pinholes in the optical path that exclude most of the light from the sample that is not in the focal plane of the microscope. Another contribution to the high resolution is point-by-point illumination. Due to the pinhole only a small point of the sample is illuminated at the time, reducing the effect of fluorescent light from other regions of the sample. The laser light scans over the surface and puts together the points to obtain the complete image.[52,53]

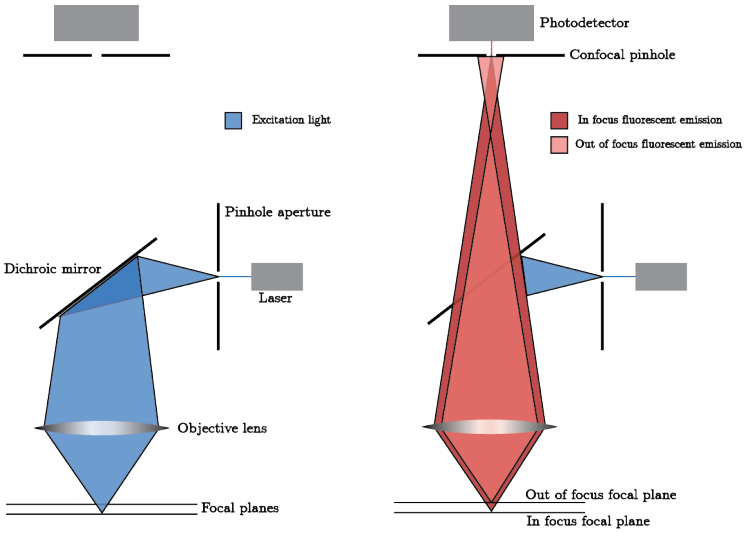

Figure A.4: Schematic representation of a confocal fluorescence microscope setup. The sample is excited by laser light. The fluorescence is then collected by the objective lens. The scattered excitation light is cut off by a dichroic mirror. Pinholes in the optical path ensure that only in-focus light is detected. Based on ref. [citenumStavitski2007].

Confocal fluorescence microscopy can be used in several ways. In this study it is used either for *ex-situ* analysis of spent technical catalysts or for *in-situ* staining experiments to visualize the active sites in fresh technical catalysts. In the first case coke species formed during the reaction are used as fluorescent probes. Upon excitation these species emit fluorescent light, thereby making it possible to map the regions in which polyaromatics are present.[54] Depending on the nature of the coke species, the emission wavelength shifts. In general, alkylated benzenes (1 ring) show fluorescence below 450 nm, naphthalenes (2 rings) and anthracenes (3 rings) between 450 and 550 nm and polyaromatics (4^+ rings) show fluorescence above 550 nm. It is therefore possible to determine the nature of the coke. Finally, it is important to keep in mind that if the coke becomes more graphitic instead of polyaromatic, fluorescence will no longer be visible, as the coke will adsorb most of the light.[55]

During *in-situ* staining experiments, the fresh technical catalysts are stained with probe molecules, for example to visualize the active sites or pore accessibility. In this study, the catalysts are stained with a solution of resorcinol and phthalic anhydride that react to form the fluorescent probe fluorescein upon temperature increase, following the reaction scheme shown in Scheme A.5. As this reaction is catalyzed by both Lewis and Brønsted acid sites, all types of acid sites present in the studied catalyst will be visualized.[21,52,56,57]

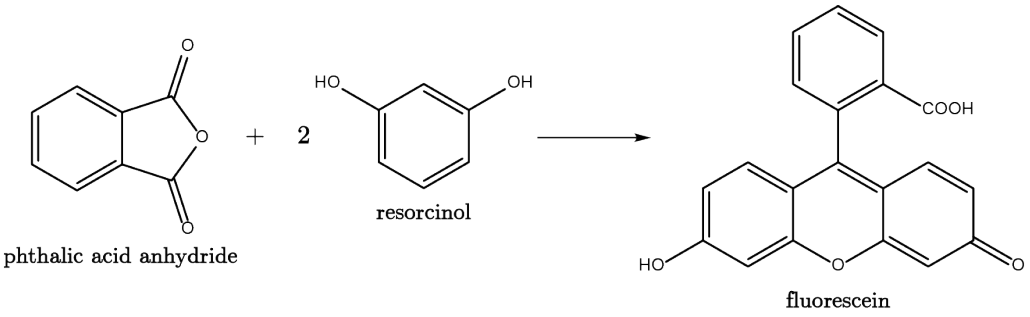

Scheme A.5: Reaction scheme of the *in-situ* synthesis of fluorescein using phthalic acid anhydride and resorcinol. Adapted from ref. [57].

Appendix B

Complementary results

In this chapter experimental data referred to in Chapter 3 are shown.

B.1 Catalytic performance

Here, the additional experimental data obtained during *operando* measurements combined with on-line MS and *in-situ* measurements combined with off-line GC can be found.

B.1.1 On-line MS

In Figure B.1, B.2 and B.3 the MS data obtained during *operando* experiments combined with on-line MS using K-USY, K-(USY/Attapulgite), attapulgite, K-(USY/Bentonite) and bentonite as catalysts is shown. Additionally, in Figure B.4 a comparison between the ratio of product intensities at t = 55 minutes for each catalyst material is shown.

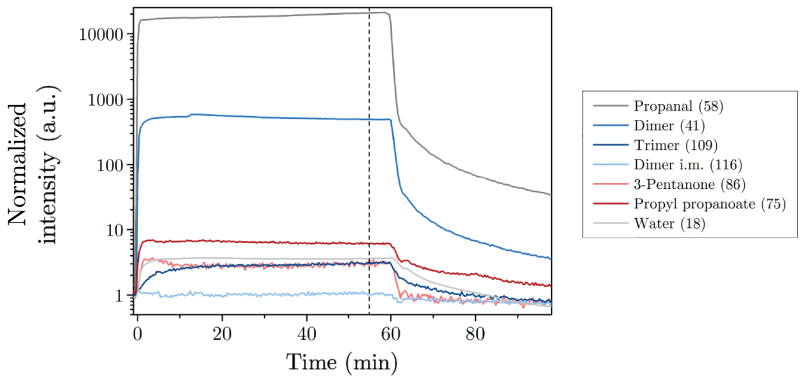

Figure B.1: On-line MS data obtained during the gas-phase conversion of propanal and subsequent desorption at 400 °C over K-USY. The experimental data was normalized by the carrier gas signal (N_2, $\frac{m}{z} = 28$), the initial signal intensity and the catalyst weight. The dashed line indicates t = 55 min, from which the intensity ratio of the products is determined.

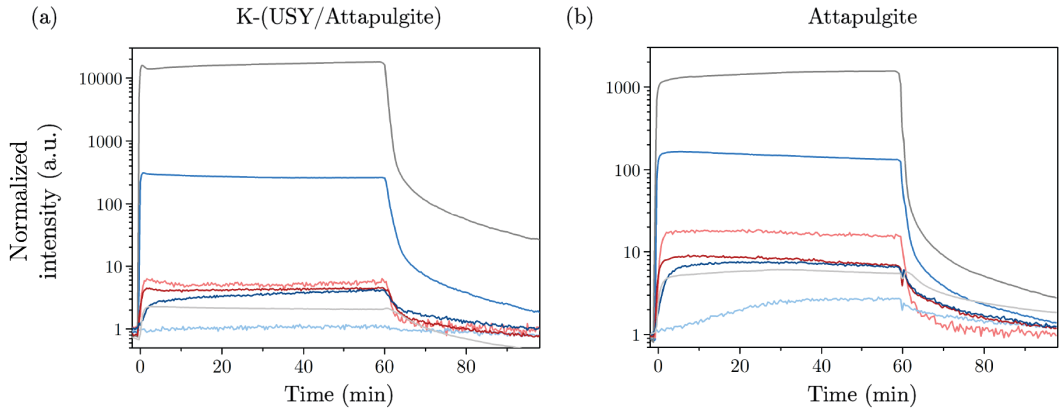

Figure B.2: On-line MS data obtained during the gas-phase conversion of propanal and subsequent desorption at 400 °C over (a) K-(USY/Attapulgite) and (b) attapulgite. The experimental data was normalized as explained in Fig. B.1 and the same legend applies here.

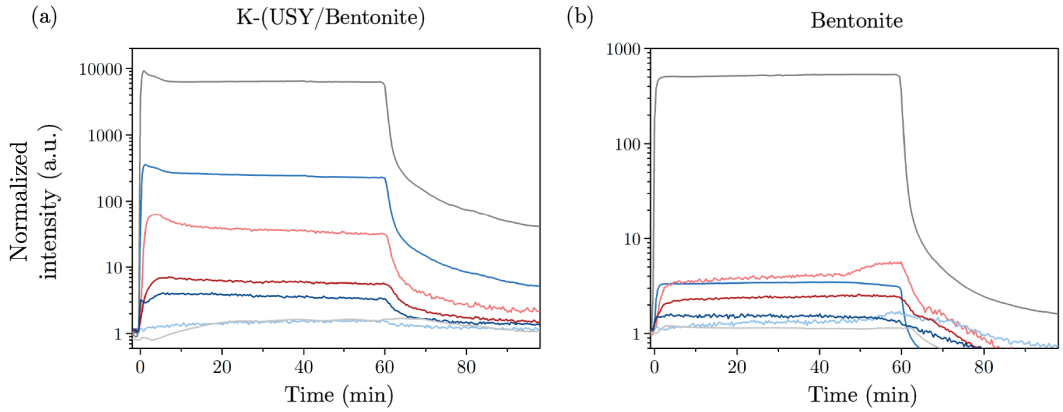

Figure B.3: On-line MS data obtained during the gas-phase conversion of propanal and subsequent desorption at 400 °C over (a) K-(USY/Bentonite) and (b) bentonite. The experimental data was normalized as explained in Fig. B.1 and the same legend applies here.

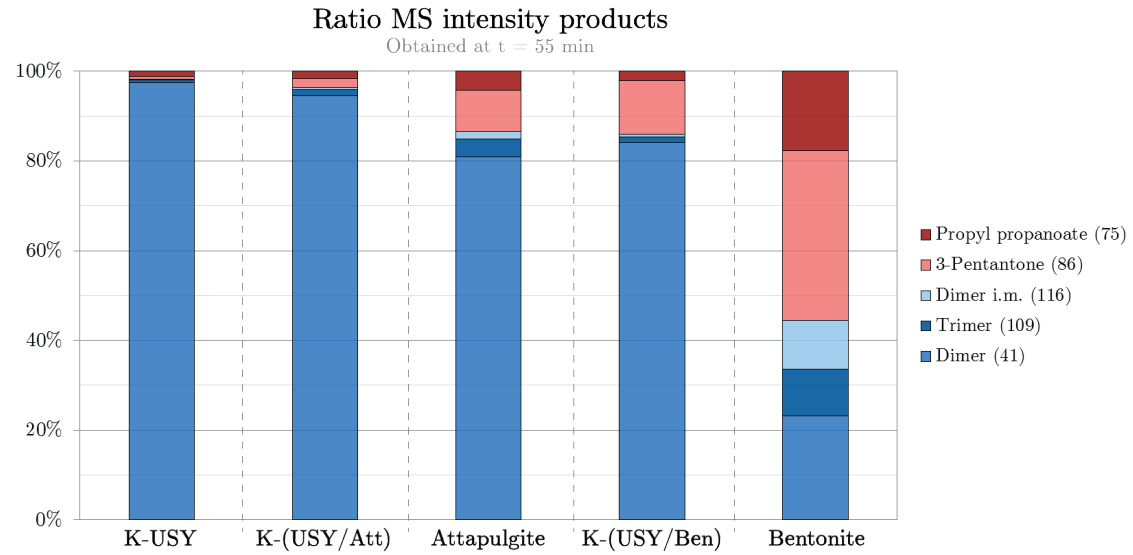

Figure B.4: Comparison of the ratio in $\frac{m}{z}$-signal intensity of the reaction products determined at t = 55 min for the gas-phase conversion of propanal over K-USY, K-(USY/Attapulgite), attapulgite, K-(USY/Bentonite) and bentonite.

B.1.2 In-situ UV-VIS spectroscopy

In Figure B.5, B.6 and B.7 the UV-Vis spectra obtained during *operando* or *in-situ* experiments using K-USY, K-(USY/Attapulgite), attapulgite, USY/Bentonite, K-(USY/Bentonite) and bentonite as catalysts are shown.

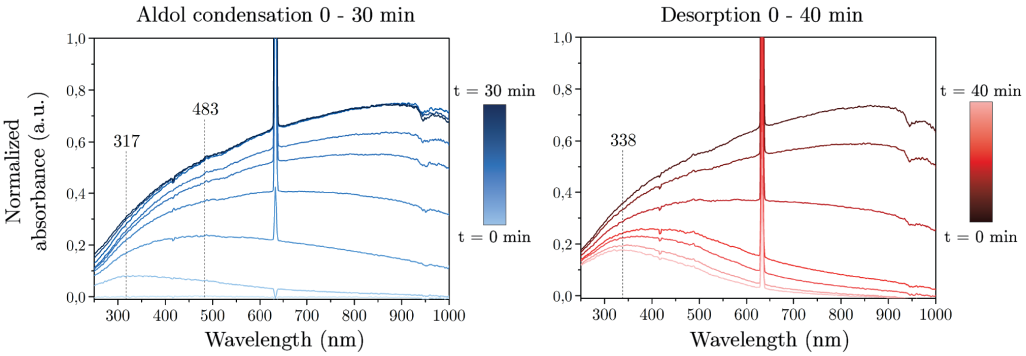

Figure B.5: Normalized DRS-UV-Vis absorbance spectra obtained during the gas-phase conversion of propanal and subsequent desorption at 400 °C over K-USY.

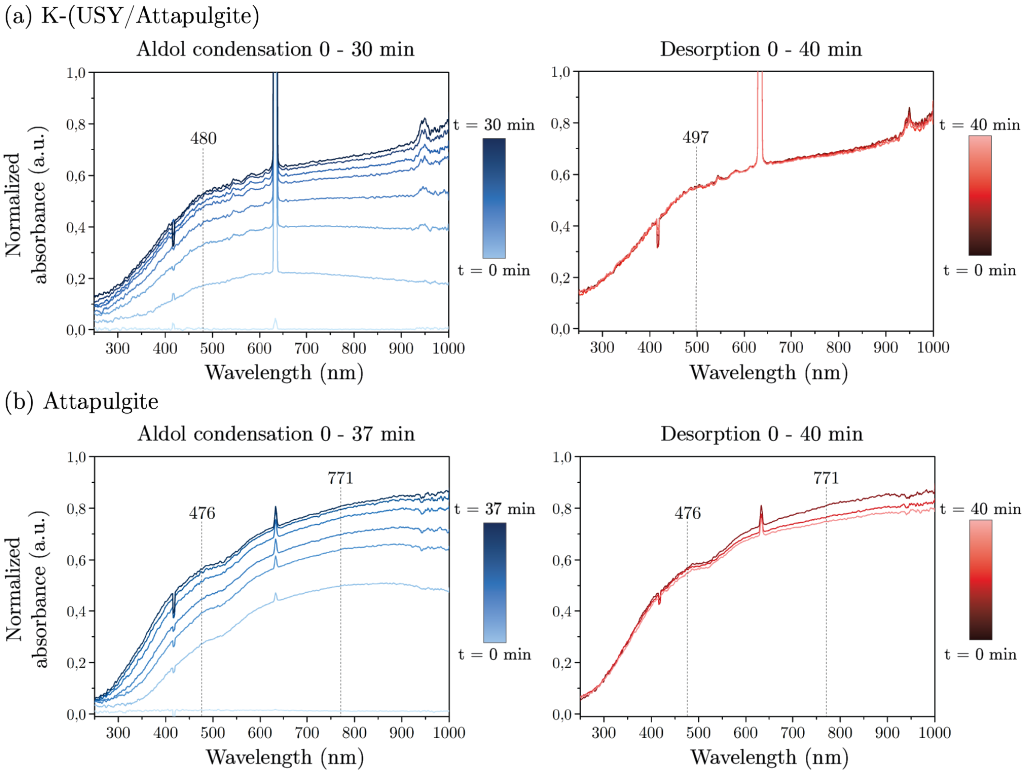

Figure B.6: Normalized DRS-UV-Vis absorbance spectra obtained during the gas-phase conversion of propanal and subsequent desorption at 400 °C over (a) K-(USY/Attapulgite) and (b) attapulgite.

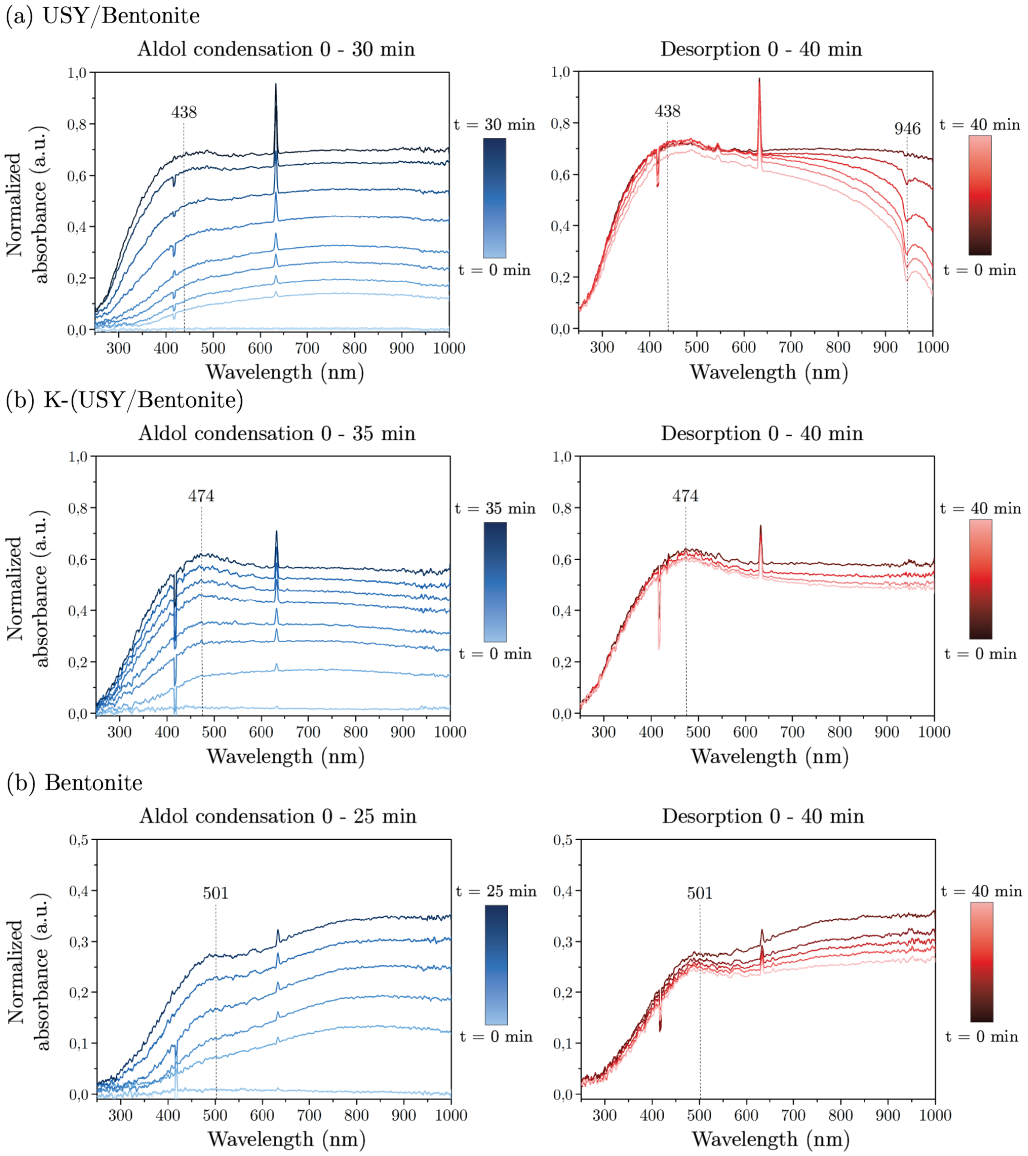

Figure B.7: Normalized DRS-UV-Vis absorbance spectra obtained during the gas-phase conversion of propanal and subsequent desorption at 400 °C over (a) USY/Bentonite, (b) K-(USY/Bentonite) and (c) bentonite.

B.2 Long term stability K-grafted USY

In section 3.1 it was discussed that the K-grafted USY research catalyst was not stable over a long time. As a result of zeolite framework degradation, loss in crystallinity, surface area and pore volume was observed with XRD and Ar physisorption measurements. In Figure B.8 the XRD diffractograms are shown. The reduction in peak intensity, broadening of the peaks and broad amorphisation peaks (5-15 and 20-35 $2\theta^{\circ}$) indicate a large loss in crystallinity. This is confirmed by the loss in surface area and pore volume observed by Ar physisorption, as shown in Table B.1.

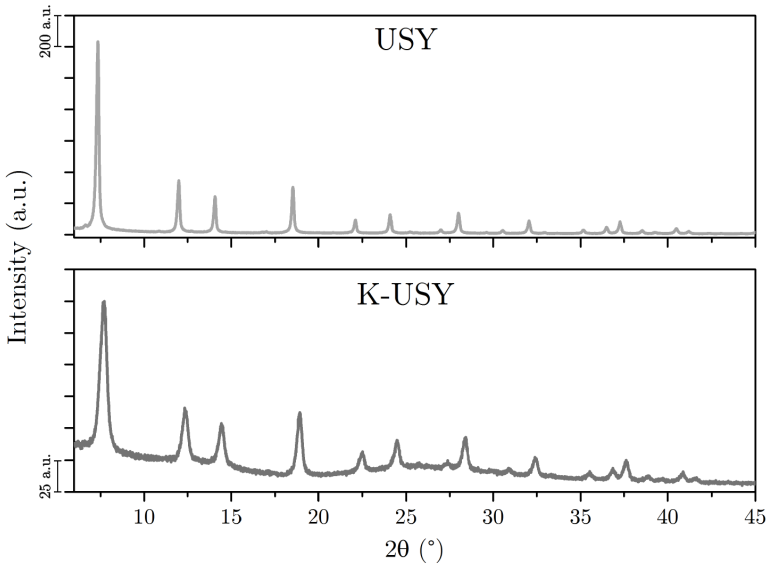

Figure B.8: XRD patterns of USY and K-USY in the region between 6 and 45 $2\theta^{\circ}$.

Table B.1: Results from physisorption analysis on USY and K-USY.

Catalyst	S_{BET} (m^2 g^{-1})	V_{pore} (cm^3 g^{-1})	$V_{micropore}$ (cm^3 g^{-1})
USY	755.8	0.384	0.259
K-USY (2015)[a]	590	0.51	0.27
K-USY (2017)	187.2	0.141	0.060

[a] Obtained by Keller et al. using N_2 physisorption.[19]

B.3 Active sites

In Figure B.9 the CO_2-IR absorbance spectra of bentonite in the region between 1800 and 1300 cm^{-1} with increasing CO_2 pressure are shown.

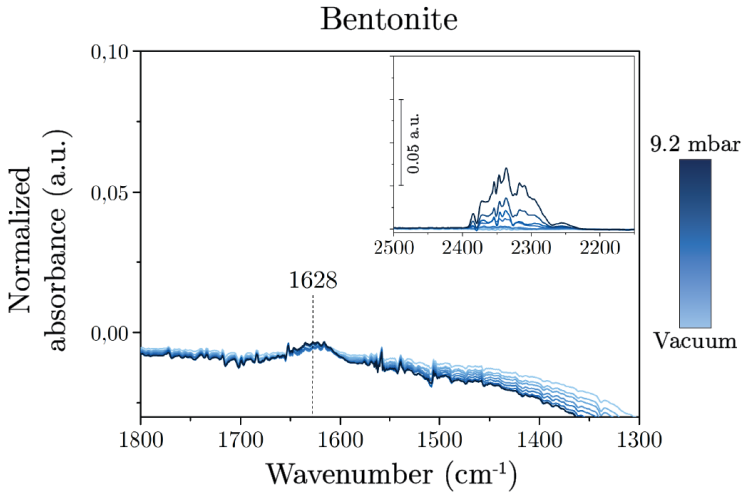

Figure B.9: Normalized FT-IR spectra of bentonite during CO_2 adsorption at room temperature.

B.4 Composition clay

Using ICP-OES the composition of attapulgite and bentonite was determined. In Table B.2 the results are shown. Trace elements present in less than 0.5 wt% in both clays are not shown in the Table. These include Ba, Cr, Ga, Mn, Ti and V for attapulgite and Mn, S, Sr, Ti, V and Zr for bentonite.

Table B.2: Elemental composition attapulgite and bentonite as determined by ICP-OES.

Element	wt% in attapulgite	wt% in bentonite
Al	4.96	10.60
Ca	1.36	-
Fe	2.73	2.78
K	0.58	0.45
Mg	2.62	1.44
Na	0.06	1.40
P	2.82	0.02
Si	34.7	N.A.